Increasing excitation vs. decreasing inhibition in auditory cortex: Consequences on the discrimination performance between communication sounds

Quentin Gaucher, Pierre Yger, Jean-Marc Edeline

DOI: 10.1113/JP279902

Increasing excitation vs. decreasing inhibition in auditory cortex: Consequences on the discrimination performance between communication sounds

Quentin Gaucher[1,2,*], Pierre Yger[3], Jean-Marc Edeline[1,2]

Paris-Saclay Institute of Neurosciences (Neuro-PSI)
Department Cognition and Behavior
[1] CNRS UMR 9197, [2] Université Paris-Sud, Bâtiment 446,
91405 Orsay cedex, France
[3] Institut de la Vision, INSERM UMRS 968, UPMC UM 80, CNRS UMR 7210, Paris, France

Running Title: Reducing intra-cortical inhibition vs. increasing excitation

Key words: Cortical excitability, discrimination between communication sounds, spike-timing reliability.

Table of contents category: Neuroscience

Correspondance to
Jean-Marc Edeline
Paris-Saclay Institute of Neuroscience (Neuro-PSI)
UMR CNRS 9197, Université Paris-Sud, Bâtiment 446,
91405 Orsay cedex, France
Email: jean-marc.edeline@u-psud.fr

* Present address: Department of Physiology, Anatomy and Genetics, University of Oxford, Oxford OX1 3PT, United Kingdom

Abstract

The level of excitability of cortical circuits is often viewed as one of the critical factors controlling perceptive performance. In theory, enhancing cortical excitability can be achieved either by reducing inhibitory currents or by increasing excitatory currents. Here, we evaluated whether reducing inhibitory currents or increasing excitatory currents in auditory cortex similarly affects the neurons' ability to discriminate between communication sounds. We attenuated the inhibitory currents by Gabazine (GBZ) application, and increased the excitatory currents by applying AMPA in the auditory cortex while testing frequency receptive fields and responses to communication sounds. GBZ and AMPA enlarged the receptive fields and increased the responses to communication sounds to the same extent. The spike-timing reliability of neuronal responses was largely increased when attenuating the intracortical inhibition but not after increasing the excitation. The discriminative abilities of cortical cells increased in both cases but this increase was more pronounced after attenuating the inhibition. The shape of the response to communication sounds was modified in opposite direction: Reducing inhibition increased the post-excitation suppression whereas this suppression tended to disappear when increasing the excitation. A computational model indicates that the additive effect promoted by AMPA vs. the multiplicative effect of GBZ on neuronal responses, together with the dynamics of spontaneous cortical activity, can explain these differences. Thus, although apparently equivalent for increasing cortical excitability, acting on inhibition vs. on excitation impacts differently the cortical abilities to discriminate natural stimuli, only modulating inhibition changed efficiently the cortical representation of communication sounds.

Key Point summary

* Enhancing cortical excitability can be achieved by either reducing intracortical inhibition or by enhancing intracortical excitation. Here we compare the consequences of reducing the intracortical inhibition and of enhancing intracortical excitation on the processing of communication sounds in the primary auditory cortex.

* Local application of Gabazine and of AMPA enlarged the spectrotemporal receptives fields and increased the responses to communication to the same extent. The Mutual Information (an index of the cortical neurons' ability to discriminate between natural sounds) was increased in both cases, and so were the noise and signal correlations.

* The spike-timing reliability was only increased after GBZ application and the post-excitation suppression was affected in opposite way: it was increased when reducing the intracortical inhibition but eliminated by enhancing the excitation.

* A computational model suggests that these results can be explained by an additive effect vs a multiplicative effect

Abbreviations List

AMPA : α-amino-3-hydroxy-5-methyl-4-isoxazolepropionic acid
GBZ : Gabazine
MGB: Medial Geniculate Body
MI : Mutual Information
PSTH : Peristimulus Time Histogramme
STRF : Spectro Temporal Receptive Field
TBOA : DL-threo-beta-Benzyloxyaspartate

Introduction

In any sensory modality, the interplay between synaptic excitation and inhibition - the two driving forces at play in cortical networks - sculpts the functional properties of cortical cells (Swadlow, 2003; Oswald *et al.*, 2006; Isaacson & Scanziani, 2011; Xue *et al.*, 2014; Moore *et al.*, 2018). In auditory cortex (ACx), it has long been debated whether synaptic inhibition is co-tuned with excitation (Wehr & Zador, 2003; Froemke *et al.*, 2007; Tan & Wehr, 2009; Moore & Wehr, 2013) or mostly acts as lateral inhibition (Wu *et al.*, 2008; Li *et al.*, 2019; Liang *et al.*, 2019) and these two configurations might coexist because different types of cortical interneurons can be involved in generating either co-tuning (Moore & Wehr, 2013) or lateral inhibition (Li *et al.*, 2019). Compelling evidence has pointed out that the relationship between excitation and inhibition is tightly controlled in such a way that any change in one of these two components is compensated by change in the other (Turrigiano & Nelson, 2000, 2004; Hensch & Fagiolini, 2005; Moore *et al.*, 2018; Briguglio *et al.*, 2018). In other words, the excitation/inhibition balance is strictly regulated despite fluctuating levels of cortical activity and despite a large diversity of situations triggering experience-dependent cortical plasticity (review in Nelson & Turrigiano, 2008; Debanne & Poo, 2010; Yizhar *et al.*, 2011). The ultimate goal of this highly precise interplay between excitation and inhibition is probably to provide a fast and efficient way for identifying and discriminating between natural stimuli (review in Gaucher *et al.*, 2013; Wang, 2018).

Recently, several studies have modified the excitation/inhibition balance by optogenetic manipulations while testing sound evoked responses. For example, suppressing the activity of parvalbumine positive (PV+) inhibitory interneurons in layer IV using archaerhodopsin produced an increase in firing rate in pyramidal cells, but paradoxically also led to an increase of both excitation and inhibition to pyramidal cells downstream of layer IV (Moore *et al.*, 2018). This result suggests that manipulating PV+ interneurons can have profoundly different consequences for pyramidal cells depending on their relative position in cortical circuit. Also, it was observed that optogenetically manipulating PV+ in the auditory cortex of behaving mice can induce correlated changes in neurometric and behavioral threshold (Briguglio *et al.*, 2018). However, suppressing PV+ produced either an increase or no change in the behavioral frequency discrimination threshold; and activating PV+ cells led to a decrease threshold for some animals and an increase for others. This variability of the optogenetic manipulations on the cortical and behavioral thresholds may stem from the type of pyramidal cells which were impacted by the activation/suppression of PV+ cells, as suggested by the Moore *et al.* (2018) study. Therefore, although optogenetic activation is a very powerful tool, it also leads to variable consequences on cortical circuits.

Very few attempts have been made to determine if changing the excitation/inhibition balance alters the abilities of ACx neurons to discriminate between natural stimuli. Disrupting intracellularly $GABA_A$ inhibition, Rosen & Mooney (2003) reported that there was little effect on the temporal organization of the neuronal responses to the bird's own song in zebra finch HVC neurons. In contrast, blocking $GABA_A$ receptors in the bird functional analog of the non-primary ACx (the NCM nucleus) increased the phasic components of responses to conspecific songs (Pinaud *et al.*, 2008). In guinea-pig primary ACx, we previously reported that a partial blockage of intracortical inhibition by brief application of

Gabazine (GBZ, a potent antagonist of $GABA_A$ receptors) enhanced the discriminative abilities of ACx neurons (Gaucher *et al.*, 2013*a*).

Here, we compare the discrimination performance of ACx neurons under two conditions of increased cortical excitability. In the first case, the increased excitability was induced by a global non-specific attenuation of the intracortical inhibition via GBZ application. In the second case, a global increase in neuronal excitability was promoted by AMPA application, which directly depolarize all cortical neurons. We first assessed the consequences of these two manipulations on the spectro-temporal receptive fields (STRFs) of cortical neurons, then we evaluated the responses to a set of conspecific vocalizations during the period of enhanced cortical excitability and quantified the discriminative abilities of ACx neurons. Although the consequences of these two manipulations gave similar results when neuronal responses were tested with pure tones, they differed in some respects when tested with vocalizations. A computational model was implemented to better understand the mechanisms underlying the differences between the effects triggered by GBZ and AMPA applications. This model suggested that the additive effect of AMPA vs. the multiplicative effect of GBZ on the synaptic gain, explains the different impacts on the temporal organization of response to communication sounds.

Materials and Methods

The methods were the same as our previous studies (Gaucher *et al.*, 2013*a*; Gaucher & Edeline, 2015) and are summarized below.

Subjects

Recordings were made in the primary ACx of adult pigmented guinea pigs of either sex. Animals, weighting from 450g to 950g (3 to 7 months old), came from our own colony with free access to food and water and a 12 h light/dark cycle. All experiments were conducted in accordance with the guidelines established by the European Communities Council Directive (2010/63/EU Council Directive Decree), which are similar to those described in the *Guidelines for the Use of Animals in Neuroscience Research of the Society of Neuroscience*. The protocol was approved by the ethical committee Paris-Sud and Centre (CEEA N°59, project N° 2014-22). The animal's audiogram was determined 2-3 days before the experiment by testing auditory brainstem responses (Echodia system, RTLab) under isoflurane anaesthesia (2.5%). All the animals used here showed audiograms in the range previously reported for healthy guinea pigs (Robertson & Irvine, 1989; Gourévitch *et al.*, 2009; Gourévitch & Edeline, 2011).

Surgical procedures

A dose of atropine sulphate (0.06mg/kg, i.p.) was given to reduce bronchial secretions and a general analgesic (Tolfedine 1mg/kg, i.p.) was delivered. The animal was then anesthetized by an initial injection of urethane (1.2 g/kg, i.p.) supplemented by additional doses (0.5 g/kg, i.p.) when reflex movements were observed after pinching the hind paw. A local anesthetic (Xylocaine 2%) was liberally injected in the wound and a craniotomy was performed above the left temporal cortex. The dura above the auditory cortex was removed and the cerebrospinal fluid was drained through the cysterna magna to prevent oedema. A pedestal of dental acrylic cement was built to allow atraumatic fixation of the animal's head during the recording session. The stereotaxic frame supporting the animal was placed in a sound-attenuating chamber (IAC, model AC1). At the end of

the recording session, a lethal dose of pentobarbital (>200 mg/kg, i.p.) was administered to the animal.

Recording procedures

Data are from multiunit recordings collected in the primary auditory cortex (area AI). Extracellular recordings were obtained from arrays of 16 tungsten electrodes (ø: 33 µm, <1 MΩ) composed of two rows of 8 electrodes separated by 1000 µm (350 µm between electrodes of the same row). A silver wire (ø: 400 µm), used as ground, was inserted between the temporal bone and the dura mater on the contralateral side. The location of the primary auditory cortex was estimated based on the pattern of vasculature observed in previous studies (Edeline & Weinberger, 1993; Manunta & Edeline, 1999; Wallace *et al.*, 2000; Edeline *et al.*, 2001). The raw signal was amplified 10,000 times (TDT Medusa) and was then processed by an RX5 multichannel data acquisition system (TDT). The signal collected from each electrode was filtered (610-10,000 Hz) and a trigger level was set for each electrode to select the largest action potentials from the signal. The trigger level was the same before and after drug application. On-line and off-line examination of the waveforms indicated that the MUA collected here was made of action potentials generated by 3 to 6 neurons in the vicinity of the electrode. At the beginning of each experiment, we set the position of the electrode array in such a way that the two rows of eight electrodes sampled neurons responding from low to high frequency when progressing in the rostro-caudal direction (see examples of tonotopic maps in Figure 2 of Gaucher *et al.* (2012); and in Figure 2 of de Cheveigné *et al.* (2013)).

Drug delivery

Topical application has been previously used in several brain regions (Riquimaroux *et al.*, 1991, 1992; Jones & Barth, 2002; Caesar *et al.*, 2003, 2008; Yu *et al.*, 2008; Wang *et al.*, 2009*a*). This technique was used here because we aimed at assessing the consequences of an increased excitability over the whole cortical map. During drug application, neuronal responses were simultaneously sampled from 16 different locations in the primary ACx. As described in previous studies (Gaucher *et al.* 2013*a,* Gaucher & Edeline 2015), the pharmacological agents were applied via a filter paper placed at immediate vicinity of the electrode array. More precisely, standardized pieces (≈0.7x2.5mm) of filter paper immersed in the drug solution (at 38° for at least 30min before application) were delicately placed on the cortical surface under microscopic control (the filter paper was also removed under microscopic control). In a previous study (Gaucher *et al.* 2013*a*), we showed that such application protocol could generate significant effects in the supragranular and granular layers in about 2min and in all cortical layers in about 4 minutes (see figure 1 of Gaucher et al 2013). As previously described in details (Gaucher *et al.*, 2013*a*), several pilot studies were performed to determine the GBZ concentration increasing cortical activity without triggering epileptiform activity and the time course of its effect. Based on several *in vivo* studies (Darbin *et al.*, 2006; Tachibana *et al.*, 2008; Darbin & Wichmann, 2008; Wang *et al.*, 2009*b*) and our previous work, we opted for a 10µM GBZ concentration, applied for 4 minutes. In contrast, pilot studies indicated that, for AMPA application, a 4-minute application was not sufficient to reliably increase spontaneous and evoked firing rate, and therefore, we decided to use continuous application of AMPA (100µM). Figure 1 summarizes the effects that were obtained on the response strength (during tests with pure tones) with the different concentrations of GBZ and of AMPA that we have used in these pilot experiments.

In several pilot experiments, the glutamate transporter inhibitor DL-threo-beta-Benzyloxyaspartate (DL-TBOA, Tocris, see Shimamoto *et al.*, 1998) was used to reduce glutamate uptake and thus to

increase its concentration in the synaptic cleft, leading to an increase neuronal excitability. Two concentrations (1mM and 2mM) and two application protocols (4' application and continuous application) were used but we did not detect significant effects on evoked firing rates and on the STRF parameters no matter the concentration/duration of DL-TBOA used. These data will not be presented in the results section.

All drugs were freshly dissolved on the day of the experiment and kept at 38°C until application on the cortical surface.

Acoustic stimuli

Artificial stimuli: Acoustic stimuli were generated in Matlab, transferred to a RP2.1-based sound delivery system (TDT) and sent to a Fostex speaker (FE87E). The speaker was placed at 2 cm from the guinea pig's right ear, a distance at which the speaker produced a flat spectrum (± 3 dB) between 140 Hz and 36 kHz. Spectro-temporal receptive fields (STRFs) were determined using gamma-tone frequencies, covering six (0.14-9 kHz or 0.28-18 kHz or 0.56-36 kHz) or eight (0.14-36 kHz) octaves respectively and presented at 75dB SPL. Each frequency was repeated eight times at a rate of 2.35Hz in pseudorandom order. The duration of these tones over half-peak amplitude was 15 ms and the total duration of the tone was 50 ms, so there was no overlap between tones.

Natural stimuli: The set of vocalizations (three conspecific and five heterospecific) were the same as in previous studies (Gaucher *et al.*, 2013*a*; Gaucher & Edeline, 2015). The conspecific vocalizations were recorded from animals of our colony: they include a purr, a chutter and a whistle call. Three heterospecific vocalizations were selected to roughly match the conspecific vocalizations both in terms of spectral content and in terms of frequency/amplitude modulations according to visual inspection of their spectrograms. These vocalizations were a dolphin chutter, a rabbit whistle and a dove purr. Two other heterospecific vocalizations were selected to be strongly different from conspecific vocalizations and included a Marsh Warbler song and a low frequency call from a wart-biter cricket. All heterospecific vocalizations were downloaded from the Macaulay Library of the Cornell laboratory of Ornithology (see http://macaulaylibrary.org/index.do).

Experimental protocol

After inserting the 16 electrodes array in the cortical tissue, at least a 30-minutes recovering time lapse was allowed for the cortex to return to its initial shape, then the array was slowly lowered. The recording depth was 500-1000µm, which corresponds to layer III and the upper part of layer IV (Wallace & Palmer, 2007). When a clear tuning was obtained for at least 8 of the 16 electrodes, the stability of the tuning was assessed: we required that the recordings displayed at least three successive similar STRFs (each lasting 6 min) before starting the protocol. When the stability was satisfactory, the protocol started by presenting the acoustic stimuli in the following order: Gamma-tones to determine the STRF at 75dB followed by three minutes of spontaneous activity, followed by the set of vocalizations presented at 75 dB SPL. Files containing both conspecific and heterospecific vocalizations were repeated 20 times. Presentation of this entire stimulus set lasted 10 minutes. For GBZ, it was followed by the 4-minutes period of drug application, then the same set of stimuli was presented in the same order, as long as the neuronal recordings were stable (usually during 60 minutes). For AMPA application, after the pre-application test, the drug was applied and the same set of stimuli was presented repeatedly as long as the recordings were stable.

Data analysis

Quantification of responses to pure tones

The STRFs were obtained by constructing post-stimulus time histograms (PSTHs) for each frequency with 1 ms time bins. All spikes falling in the averaging time window (starting at stimulus onset and lasting 100 ms) were counted. Thus, STRFs are matrices of 100 bins in abscissa (time) multiplied by 97 or 129 bins in ordinate (frequency). For each STRF, significant responses were automatically identified using the following procedure: A peak in the STRF was defined as a contour of firing rate above the average level of the baseline activity (estimated from the first ten milliseconds of STRFs where no evoked activity can be expected) plus six times the standard deviation of the baseline activity. For each recording, three measures were extracted from the STRF peak responses: First, the "bandwidth" was defined as the sum of all peak's width in octaves. Second, the "response duration" was the time difference between the first and last spike of the significant peaks. Third, the "response strength" was the total number of spikes falling in the significant peaks.

Quantification of responses evoked by vocalizations

The responses to vocalizations were quantified using two parameters: (i) The evoked response, which corresponds to the difference between evoked and spontaneous firing rates at presentation of the vocalizations and (ii) the spike-timing reliability coefficient (CorrCoef) which was used to quantify the response trial-to-trial reliability. This index was computed for each vocalization: it corresponds to the normalized covariance between each pair of action potential trains recorded at presentation of this vocalization and was calculated as follows:

$$CorrCoef = \frac{1}{N(N-1)} \sum_{i=1}^{N-1} \sum_{j=i+1}^{N} \frac{\sigma_{x_i x_j}}{\sigma_{x_i} \sigma_{x_j}}$$

where N is the number of trials and $\sigma_{x_i x_j}$ is the normalized covariance at zero lag between spike trains x_i and x_j where i and j are the trial numbers. Spike trains x_i and x_j were first convolved with a 10 ms width Gaussian window. This value was chosen according to the analysis of the temporal precision maximizing the Mutual Information (MI). The CorrCoef is not influenced by the firing rate, and had a chance value of 0.026 for a 0.01 confidence interval (Gaucher *et al.*, 2013*a*; Gaucher & Edeline, 2015).

To discard recordings not responding to any vocalization, we set up a criterion of an evoked firing rate of at least 1.5 spike/s or a CorrCoef of at least 0.15. A systematic and meticulous examination of our database has shown that recordings exhibiting only a phasic onset response generated a CorrCoef of at least 0.15, and that cells responding by tonic responses lacking of temporal organization generated at least a firing rate of 1.5 spike/s.

Quantification of mutual information from the responses to vocalizations.

We used an indirect method to quantify the amount of information (Shannon, 1948) contained in the responses to vocalizations obtained before, during and after drug application (Schnupp, 2006). This method allows quantifying how well the vocalization's identity can be inferred from the neuronal responses. Neuronal responses can be represented using different time scales ranging from the whole response (firing rate) to a 1 ms precision (precise temporal patterns), which allows analyzing how much the spike timing contributes to the information. As this method is exhaustively

described in Schnupp *et al.* (2006) and in our previous studies (Gaucher *et al.*, 2013*a*; Gaucher & Edeline, 2015), we will present here only the main principles.

From the responses of a cortical site to the different vocalizations, a single response (test pattern) is extracted and represented as a PSTH with a given bin size. Then, from the remaining responses (training set), a mean response pattern is computed for each stimulus class. The test pattern is then assigned to the stimulus class of the closest mean response pattern. This operation is repeated for all the responses, generating a confusion matrix where each response is assigned to a given stimulus class. From this confusion matrix, the Mutual Information (MI) is given by Shannon's formula:

$$MI = \sum_{x,y} p(x,y) \times \log_2 \left(\frac{p(x,y)}{p(x) \times p(y)} \right)$$

where x and y are the rows and columns of the confusion matrix, or in other words, the values taken by the random variables "presented stimulus class" and "assigned stimulus class".
In our case, we used responses to the 8 vocalizations and selected the first 264ms of these responses to work on spike trains of the same duration; the shortest vocalization being 264ms long (the conspecific whistle). In a scenario where the responses do not carry any information, the assignments of each response to a mean response pattern will be equivalent to chance level (1/8 because we used 8 stimuli and each stimulus was presented the same number of times) and the MI would be close to zero. In the opposite case where responses are very different between stimulus classes and very similar within a stimulus class, the confusion matrix would be diagonal and the mutual information would tend to $\log_2(8) = 3$ bits.

This algorithm was applied at a bin sizes of 8ms, which was a temporal resolution leading to the highest values of information in previous studies (Schnupp, 2006; Huetz *et al.*, 2009; Gaucher *et al.*, 2013*a*). As in Schnupp *et al.* (2006), we estimated the expected size of this bias by calculating MI values for "shuffled" data, in which the response patterns were randomly reassigned to stimulus classes. The shuffling was repeated 100 times, resulting in 100 MI estimates of the bias (MI_{bias}). These MI_{bias} estimates are then used as estimators for the computation of the statistical significance of the MI estimate for the real (unshuffled) datasets: the real estimate is considered significant if its value is statistically different from the distribution of MI_{bias} shuffled estimates. Significant MI estimates were computed for MI calculated from neuronal responses under one electrode.

Quantification of signal and noise correlations.
To evaluate neuronal reliability at the level of pair of neurons, we performed an analysis of noise and signal correlations as described in previous studies (Averbeck & Lee, 2003; Latham & Nirenberg, 2005; Averbeck *et al.*, 2006). This method aims to dissociate between noise correlations (i.e. the firing rate correlation for a pair of neurons in response to presentations of the same stimulus) vs. signal correlation (i.e. the correlation between the mean responses of the same pair of neurons to different stimuli). Noise correlations, if present, reflect the existence of a connection between two recording sites, without making assumptions on the anatomical circuitry of this connection. They only represent a co-variation of the variability of the recording sites responses. Signal correlations reflect a co-tuning of a pair of recording sites. To compute noise correlation, the firing rate of neuronal responses to each stimulus was first normalized by the average firing rate in response to this stimulus. Then, the normalized firing rates in response to each presentation of each stimulus were taken for a pair of recordings, and the Pearson correlation coefficient between them was

computed. The values of the Pearson coefficient for each pair of recordings were then averaged. To compute the signal correlation, we computed the Pearson coefficient between the mean responses to each stimulus from a pair of recordings. We then averaged the result for all pairs of recordings.

Statistical analyses

In the text describing the physiological results, data are presented as mean values ± standard deviation (SD). In figures, summary data are represented with boxes indicating the median, 25th percentile and 75th percentiles. Unless otherwise specified, all the statistical tests are Wilcoxon signed-rank tests (as some distributions of our results differed from a normal distribution). The data that support the findings of this study are available from the corresponding author upon reasonable request.

Computational model

Neuron model

Simulations were performed using current-based leaky integrate-and-fire neurons with a membrane time constant $\tau_m = 5ms$ (Destexhe *et al.* 1999) and a resting membrane potential $V_{rest} = -70mV$. When the membrane potential V_m reaches the spiking threshold $V_{thresh} = -55mV$, a spike is generated and the membrane potential is clamped to the reset potential $V_{reset} = -70mV$ during a refractory period of duration $\tau_{ref} = 5ms$. Each presynaptic spike produces an exponential decaying current with time constant $\tau_{exc} = 3ms$ for excitation and $\tau_h = 5ms$ for inhibition. In order to have spontaneous activity, all neurons are stimulated with a white noise current $x(t)$ with mean $\mu = 0mV$ and variance $\sigma = 6mV$. The model equations are thus:

$$dV\,(t)/dt = \left(V_{rest} - V(t)\right) + g_{exc}(t) + g_{inh}h(t) + x(t)\sigma\sqrt{(2\tau_m)}$$

$$\tau_{syn}\left(dg_{syn}(t)\right)/dt = -g_{syn}(t)$$

where $syn \in \{exc, inh\}$ and each presynaptic spike produces an instantaneous increase: $g_{syn} \leftarrow g_{syn} + \lambda_{syn}w_i$ where w_i is the synaptic weight of synapse *i* and $\lambda_{syn}$is a scaling factor calculated so that a synaptic weight of 1 mV produces PSPs of peak size 1 mV. Note that $g_{syn}(t)$ is in units of volt, i.e., the membrane resistance is implicitly included in the variable. For exponential synapses, we can compute analytically that

$$\lambda_{syn} = \left(\frac{\tau_m}{\tau_{syn}}\right)^{\frac{\tau_m}{\tau_m - \tau_{syn}}}$$

Network model

We used a random balanced network composed of 4000 excitatory neurons and 1000 inhibitory neurons. Every neuron in the network is connected to 10% of the others, with delays drawn from a uniform distribution between 0 and 5 ms. To set the network in a balanced regime, we neglected the contribution of spikes and use Campbell's theorems, which give the mean and variance of a shot noise (corresponding to sums of PSPs with Poisson statistics):

$$< V_m >= FN_{exc}w_{exc} < \int EPSP > + FN_{inh}w_{inh} < \int IPSP > + V_{rest}$$

where F is in the firing rate of the network, and N_{syn} the average number of incoming synapses per neuron. In the balanced regime, we want to have $< V_m > = V_{rest}$, so we should have

$$w_{exc}N_{exc} < \int EPSP > = -w_{inh}N_{inh} < \int IPSP >$$

Since the connection probability is uniform, we have $N_{exc} = 4N_{inh}$. Using the fact that $< \int EPSP > = \lambda_{exc}\tau_{exc}$ and $< \int IPSP >= \lambda_{inh}\tau_{inh}$, we have the following equation for the balance $g = w_{inh}/w_{exc}$

$$g = \frac{-4\tau_{exc}\lambda_{exc}}{\tau_{inh}\lambda_{inh}} = -1.2\frac{\lambda_{exc}}{\lambda_{inh}}$$

Initial synaptic weights for recurrent excitatory connections are drawn from a Gaussian distribution with mean 0.2 mV and standard deviation equal to a fourth of the mean. To be in a strong balanced regime, recurrent inhibitory connections are drawn from a Gaussian distribution such that $< w_{inh} >= -1.5g < w_{exc} >$ (standard deviation of the Gaussian distributions are also chosen to be a fourth of the means).

Thalamic inputs

Each neuron in the network receives inputs from 8 groups of 100 neurons each, with a connection probability of 10%. In each of those groups, inputs are independent inhomogeneous Poisson sources all driven by a common fluctuating input (one per group). The inputs are generated as rectified Orstein-Ulbheck noises with temporal correlations of $\tau_{noise} = 50ms$, and a maximal amplitude of 100Hz. Such a simulated network is similar to the one described by Vogels and colleagues (2011).

Generation of Multi-Unit activity

To take into account the fact that the experimental data are not Single Unit (SU) (no spike sorting was performed), we generated Multi-Unit Activity (MUA) out of the activities in the balanced network. To do so, we randomly selected between 1 and 5 neurons within the network, and pooled their activities together to obtain a "simulated" MUA. Note that the main effect of such a transformation is mostly to affect the firing rates of the "units", but qualitatively, all the results shown in the paper still hold when the analysis is performed at the level of the individual neurons (data not shown). In all the simulations, results are averaged over a population of 100 simulated multi-units constructed from the activities of the individual neurons as described above.

AMPA and Gabazine effects

In the model, the influence of AMPA injection is considered to be additive, i.e. resulting in a constant excitatory current injected into all neurons (both excitatory and inhibitory) to reflect the fact that the actual AMPA application affects both active and inactive excitatory synapses. The strength of that external input was arbitrarily set to 5mV. On the contrary, the effect of GBZ is considered to be multiplicative, because the drug only affects inhibitory synapses that are activated. Therefore, in the model, this is taken into account by a multiplicative scaling of the inhibitory weights, with a scaling factor $\alpha < 1$. In all the simulations, we used $\alpha = 0.5$, a value ensuring that both AMPA and Gabazine would have similar effect on the mean firing rate of the neurons during spontaneous activity.

Reproducibility

The correlations between trials or between neurons have been computed exactly with the methodology used for the analysis of the *in vivo* data (namely with the CorCoeff index and the CrossCorrelation). The reproducibility was assessed by randomly selecting 100 snippets of 500ms

length from the fluctuating inputs played over the 8 groups, and repeating each of them 100 times. Those snippets were considered, in the model, as putative inputs occurring at presentation of vocalizations.

PSTHS

To reproduce the averaged shape of the PSTH observed *in vivo* in the response to vocalizations, we performed 100 repetitions of the following protocol, before averaging all responses. Synthetic "vocalizations" (inputs used in the model) were designed as follow: at each presentation of a vocalization, four random groups among the eight groups stimulating the neurons was selected, and the activity within these four groups was set, for a duration drawn randomly between 50 and 100ms to an inhomogeneous Poisson rate of mean 100Hz and variance 50Hz, while all other groups remained silent.

Results

Data are from 128 multi-unit recordings obtained in the primary auditory cortex of 7 guinea pigs before and after AMPA application, and from 70 recordings obtained in 5 guinea-pigs before and after GBZ application. All these recordings displayed both significant STRFs and reliable responses to at least one of the eight vocalizations (i.e. displayed a CorrCoeff value of at least 0.15 or an evoked firing rate of 1.5 spike/s above spontaneous rate, see Methods).

Consequences of GBZ and AMPA application on STRF parameters.

Confirming results from a previous study (Gaucher *et al.*, 2013*a*), a partial blockage of the intracortical inhibition by GBZ application significantly expended the STRFs in the spectral and temporal domain. Figure 2A displays a representative example of such effect. AMPA application induced a qualitatively similar effect on the STRF (Figure 2B). Group data show that, on average, AMPA and GBZ application produced similar STRFs expansions. The STRF bandwidth was significantly increased after GBZ (1.88 ± 1.12 octave to 2.54 ± 1.61 octave, $p = 3.13 \times 10^{-5}$) and AMPA application (1.99 ± 0.98 to 2.74 ± 1.44, $p = 7.32 \times 10^{-16}$, Figure 2C). The STRF duration was also significantly increased after GBZ (25.13 ± 17.45 ms to 38.75 ± 20.73 ms, $p = 6.48 \times 10^{-5}$) and AMPA application (38.75 ± 20.73 ms to 45.13 ± 21.57 ms, $p = 6.49 \times 10^{-05}$; Figure 2D). Finally, the response strength (i.e., the number of action potentials within the STRF significant contours) was also significantly increased after GBZ (31.85 ± 29.17 spike/s to 100.77 ± 127.86 spike/s, $p = 1.76 \times 10^{-05}$) and AMPA application (72.21 ± 47.92 spike/s to 122.85 ± 81.33 spike/s, $p = 8.17 \times 10^{-20}$; Figure 2E). This increase was present from the first (12min) to the last (60min) time point tested after application ($p<0.0001$; data not shown). Thus, based on STRF quantifications, the consequence of an increased excitability triggered by AMPA application cannot be distinguished from the one induced by GBZ application: it produces similar STRF expansions.

Consequences of GBZ and AMPA application on responses to vocalizations.

As expected from above, during presentations of conspecific and heterospecific vocalizations, the evoked firing rate was increased both by GBZ and by AMPA application. The raster plots displayed in figure 3A illustrate this enhancement for two examples where the increase in evoked firing rate is quite large (140% for the GBZ application and 75% for the AMPA application) together with an increase in spontaneous activity. In these examples, the trial-to-trial reliability of the evoked responses (CorrCoeff) was increased with GBZ but not with AMPA application (from 0.44 to 0.68

with GBZ; from 0.54 to 0.54 with AMPA). Note the systematic post-excitation suppression after GBZ application, which was not always present after AMPA application, could explain this difference.

The scattergrams displaying the group data confirmed that both GBZ and AMPA increased the evoked responses (GBZ: 15.26 ± 11.62 spike/s to 25.94 ± 15.01 spike/s, $p = 1.79 \times 10^{-9}$; AMPA: 31.15 ± 33.96 spike/s to 44.30 ± 34.96, $p = 1.84 \times 10^{-14}$, Figure 3B) and the spontaneous firing rate (GBZ: 3.65 ± 3.47 spike/s to 9.48 ± 6.33 spike/s, $p = 2.19 \times 10^{-4}$; AMPA: 11.60 ± 9.05 spike/s to 17.61 ± 12.19 spike/s, $p = 1.49 \times 10^{-4}$, Figure 3C). As previously described, reducing intracortical inhibition by GBZ application also increased the trial-to-trial reliability quantified by the CorrCoef index (0.43 ± 0.20 to 0.58 ± 0.19, $p = 5.80 \times 10^{-5}$). In contrast, AMPA application did not significantly increase the CorrCoef ($p = 0.78$, Figure 3D). Note that AMPA and GBZ application enhanced the evoked firing rate to the same extent: the mean increase in evoked response (unpaired t-test; $p = 0.25$) and the distribution of the percentage of changes in evoked responses (Figure 3E) did not differ after application of the two drugs (Chi-square, $p = 0.37$).

What were the consequences of these changes on the discriminative abilities of auditory cortex neurons? To evaluate how well cortical neurons discriminate between stimuli we computed the mutual information (MI) between the set of stimuli and the set of neuronal responses. MI was computed based on the temporal patterns of discharge (see Methods). On average, the mean MI value was strongly increased after GBZ application (from 0.53 ± 0.37 to 0.73 ± 0.34 bit, $p = 4.23 \times 10^{-7}$; Figure 4A) and slightly increased after AMPA application (from 0.94 ± 0.40 to 1.04 ± 0.39 bit, $p = 5.75 \times 10^{-3}$, figure 4B). It was surprising that AMPA application increased the MI values whereas, on average, it had no effect on the CorrCoef. In fact, we should keep in mind that each MI value is based on responses to the 8 vocalizations, each one providing one value of firing rate and of CorrCoef. One possibility is that despite an unchanged mean value when averaged over 8 vocalizations, the 8 values of CorrCoeff were differentially changed by AMPA application, some being increased while the other being decreased. Figure 5A displays for each recording, the change in MI (y-axis) as a function of the 8 values of changes in CorrCoef (x-axis) corresponding to the 8 vocalizations. It appeared that for a single value of MI, the 8 values of change in CorrCoeff can notably differ, both in amplitude and direction. The example displayed on Figure 5B illustrates a case where the CorrCoeff was increased for a particular vocalization (from 0.11 to 0.38), unchanged for some vocalizations and decreased for others. For that particular recording, the mean Corrcoef value was unchanged (indicated by the black dot around zero in abscissa on Figure 5A, but the improvement of the temporal reliability for one vocalization and the overall increase in evoked firing rate were enough to increase the discriminative ability of that cortical recording (ordinate largely above zero for the black dot in Figure 5A). Note that despite having no change in average on the temporal reliability, the AMPA induced change in MI and in average CorrCoef per recording site were significantly correlated ($r = 0.361$, $p = 0.002$, Pearson correlation). In contrast with the effect of AMPA application, for a given recording the CorrCoef corresponding to the different vocalizations were all increased in a similar way after GBZ application (data not shown). To conclude, on average AMPA application did not affect the CorrCoef but it increased the MI because of its heterogeneous effect on the CorrCoef.

Key differences between the action of GBZ and AMPA

So far, the difference between the effects of AMPA and GBZ on the responses to natural stimuli is rather modest: the CorrCoeff index was increased after GBZ application but not after AMPA

application. However, analyzing the effect of the two pharmacological agents on the time course of evoked response pointed out a striking difference. In control conditions, the phasic peaks of response were often followed by a suppression of activity, potentially due to intracortical inhibition and/or to synaptic depression (Wehr & Zador, 2005). As previously noted (Gaucher *et al.*, 2013*a*), these periods of suppression were more pronounced after GBZ applications. To quantify this effect at the population level, we used a custom-made peak detector to extract peaks of activity from the PSTHs in response to vocalization. Only phasic peaks of response lasting more than 20ms and less than 80ms were selected and averaged. Figure 6A presents the averaged peaks obtained before/after GBZ (figure 6A1) and AMPA (Figure 6A2) application. The differences in firing rate before and after the peaks of response are represented in Figure 6B. Averaging all the significant peaks of responses revealed that after GBZ application, the firing rate felt below the pre-peak level whereas it remained at that level before GBZ application (pre-GBZ: from 25.5 ± 16.6 spike/s to 24.0 ± 20.4 spike/s, $p = 0.33$; post-GBZ from: 26.1 ± 18.2 spike/s to 6.8 ± 12.2 spike/s, $p = 2.34 \times 10^{-7}$; Figure 6B1). This effect was not observed after AMPA application: spontaneous and evoked activities were increased as if the whole curve – i.e. the peak of evoked responses as well as the firing rate before and after the peak - was moved upward (pre-AMPA: from 33.1 ± 32.3 spike/s to 37.8 ± 34.5 spike/s, $p = 0.19$; post-AMPA: from 52.2 ± 36.4 spike/s to 61.5 ± 45.2 spike/s, $p = 0.03$; Figure 6B2).

Thus, despite similar effects on spontaneous and evoked firing rates, applying an antagonist of $GABA_A$ receptors paradoxically reinforced the post-excitation suppression occurring during presentation of natural stimuli, whereas increasing the activation of AMPA receptors only increased the firing rate during and between presentations of natural stimuli. One possibility is that these opposite effects stem from differences in synchronization between cortical neurons: controlling intracortical inhibition might increase the synchronization of cortical discharges, whereas controlling excitation might leave synchronization unchanged. To assess this hypothesis, we computed cross-correlations between simultaneously recorded neuronal activities. As already observed in a previous study (Gaucher *et al.*, 2012), the maximal cross-correlation was always found at 0 ms lag, indicating that the synchronized firing between different recording sites depends upon common cortical and/or thalamic inputs. When computed from all the spike-trains simultaneously collected, the mean value of cross-correlation was largely increased after GBZ application (0.073 ± 0.043 to 0.095 ± 0.039, $p = 4.63 \times 10^{-9}$; Figure7A), whereas it was slightly increased by AMPA application (0.053 ± 0.030 to 0.059 ± 0.029, $p = 5.69 \times 10^{-8}$; Figure7B). The increase in cross-correlations was significantly stronger after GBZ application than after AMPA application ($p = 1.82 \times 10^{-7}$). This result suggests that reducing intra-cortical inhibition largely increased the synchronization between discharges of cortical neurons, whereas reinforcing excitation had a less pronounced effect. This increased synchronization might be responsible for the stronger post-excitation suppression after GBZ application, an effect not observed after AMPA application.

To further understand the influence of both drugs on the correlations between neuronal responses, we computed the signal and noise correlations between pairs of cortical neurons (see Methods). Both GBZ and AMPA significantly increased the signal correlations, although the increase was stronger after GBZ application (AMPA: from 0.22 ± 0.48 to 0.33 ± 0.45, $p = 6.87 \times 10^{-9}$; GBZ: from 0.46 ± 0.41 to 0.77 ± 0.27, $p = 1.02 \times 10^{-13}$; Figure 7C). This result indicates that both drugs promoted neuronal responses to vocalizations which are, on average, more similar between each pair of neurons. As shown in Figure 7D, AMPA application slightly increased the average noise correlation level, indicating a relatively low influence of this drug on the level of covariation of activity (from

0.25 ± 0.18 to 0.28 ± 0.21, p = 0.048). On the contrary, GBZ induced a large increase in noise correlation, confirming the influence of this drug on the strength of common inputs onto pairs of neurons (from 0.31 ± 0.19 to 0.45 ± 0.29, $p = 2.83 \times 10^{-6}$). This indicates that when cortical inhibition is reduced, every pair of neurons shows similar fluctuation of activity at a given time. The difference between GBZ and AMPA lies in the fact that reducing cortical inhibition makes cortical cells responses more similar on a trial-to-trial basis, whereas increasing the cortical excitation had almost no effect on the co-variations of neuronal activities. Altogether, these results suggest that GBZ had an additional effect on the temporal structure of cortical activity that was not present after AMPA application.

Exploring potential mechanisms by a computational model

We implemented a computational model to determine which mechanisms can explain why the temporal structure of evoked responses was differentially affected by AMPA and GBZ. More precisely, we designed a simple recurrent model with spiking neurons able to reproduce our observations (see Methods). We used an already existing model (Vogels *et al.*, 2011), made of current-based spiking neurons in a balanced regime, receiving both excitatory and inhibitory inputs. Conceptually, the external inputs impinging the simulated cortical neurons reflect the feed-forward drive originating from the thalamus (MGB) (see Materials and Methods, Figure 8A). The addition of AMPA was modeled by the addition of a constant excitatory current onto all neurons, whether they were excitatory or inhibitory. On the contrary, the effect of the GBZ was modeled by a multiplicative effect, affecting only the active inhibitory synapses (Figure 8B). The assumption behind the model was that AMPA diffuses locally, affecting all synapses, whether they are activated or not. On the contrary, GBZ only affects inhibitory synapses that are activated by sensory inputs, reducing their efficacies. Therefore, the net effect of GBZ is to scale down, in a multiplicative manner, the total amount of inhibition received by the neurons. In the spontaneous regime, the network displays an asynchronous irregular regime characterized by a low firing rate (2.75 Hz; see Figure 8C), and an average coefficient of variation for the inter-spike intervals close to 1 (see inset in Figure 8C).

In all the following, in order to establish a better comparison between the results obtained with the network and the experimental data, we pooled the individual responses of randomly chosen small groups of neurons (2-5) in the network in order to generate pseudo Multi-Units activities (see Methods). While this transformation had overall no effect qualitatively on the results, it affected the global firing rates of the units. To assess the temporal reliability of the responses, we stimulated several times the neuronal network with fixed temporal patterns displaying a temporal organization similar to those of the vocalizations used in the physiological experiment (as shown in Figure 3A, see Methods). Three situations were considered. First, a control case with a fixed balance between excitation and inhibition, obtained after convergence of the system to a properly balanced regime (see Methods). Second, a perturbed regime mimicking the application of AMPA by addition of a constant current to all cortical neurons. Third, a perturbed regime mimicking the application of GBZ by scaling multiplicatively all inhibitory synapses in the model. As shown in Figure 9A, the firing rate of neurons was largely increased when the balance between excitation and inhibition was perturbed by the use of AMPA or GBZ. This is in line with the experimental increase of firing rate visible in Figures 3B1 and 3B2. As presented on Figure 9B, and similarly to what has been observed experimentally (Figure 3D), the temporal reliability measured by the CorrCoeff was higher after GBZ application that after AMPA application. In addition, the cross-correlations of spike trains were much larger with GBZ than with AMPA (Figure 9C), as was the case in our physiological data (Figure 7A and

B). Figure 9D illustrates this effect with rasterplots of simulated neurons during control (black) AMPA (blue) and GBZ conditions (orange). Most likely, this was the consequence of the additive effect of the AMPA which amplifies the responses to both stimulus and noise, while the multiplicative effect of GBZ enhances the responses to transient inputs and thus favors synchronous firing of the neurons.

So far, this minimalist model reproduced our main effect: GBZ induced an increase in temporal reliability during vocalizations whereas AMPA did not. However, another key observation was the difference in temporal response pattern obtained after GBZ and AMPA application (Figure 6). Assuming that the thalamic inputs were unchanged during drug application in cortex, this effect on the temporal response patterns should necessarily originate from intracortical connections. As displayed in Figure 9E, in the simulated network the application of GBZ and AMPA increased the spontaneous and evoked activity, while the baseline activity was kept constant. However, the increase in evoked activity was more pronounced with GBZ than with AMPA application. In addition, whereas in control conditions (black line) and AMPA conditions (blue line) the synchronous volleys of spike-locked responses were followed by brief periods of post-excitation suppression, the stronger excitatory response obtained in GBZ conditions (orange line) was followed by a much longer post-excitation suppression. This has to be contrasted with the global shift of the response to the vocalizations observed with AMPA (blue line).

To summarize, our model indicates that the difference between the effect on the CorrCoef and neuronal synchronization can be mimicked by a computational model of a thalamocortical feedforward balanced network. Using a balanced network of integrate and fire neurons, experimental findings can be recovered qualitatively when the perturbation of the balance leading to an increase of excitation is implemented either as an additive (AMPA) or a multiplicative effect (GBZ).

Discussion

We compared the consequences of an increase in neuronal excitability induced either by reducing $GABA_A$-mediated inhibition, or by increasing the AMPA-mediated excitation, on the discriminative abilities of auditory cortex neurons. When quantifying spectro-temporal receptive fields of multi-unit recordings, these two manipulations promoted similar results. In contrast, when quantifying the responses to natural stimuli, noticeable differences emerged. First, the spike-timing reliability was largely increased after attenuating intracortical inhibition whereas it was not affected after enhancing excitation. Mutual information was increased in both cases but this increase was much larger when attenuating intracortical inhibition. The temporal decay of neuronal responses strikingly differed after application of these two pharmacological agents. After GBZ application, each strong phasic peak of response was followed by a prolonged period of silence, whereas AMPA application prolonged the response duration and did not favor the occurrence of a post-excitation suppression. A computational model of the cortical network was able to replicate qualitatively these results and indicated that some of the differences between the effects triggered by AMPA and GBZ can be explained by the impact of additive vs. multiplicative effects on synaptic inputs.

Methodological considerations.

To manipulate excitation or inhibition over the whole tonotopic map, AMPA and GBZ were directly applied on the cortical surface at a given concentration. In a previous study, topical application was also used to evaluate the consequence of activating NA receptor subtypes on the discriminative performance of ACx neurons. Despite this relatively crude method, we were able to dissociate between the activation of α1, α2, and β receptors (Gaucher & Edeline, 2015) and to observe a pharmacological profile identical to the one previously described with iontophoretic application (Manunta & Edeline, 1997), suggesting that this mode of application generates results compatible with well-known physiological effects. Direct application of AMPA in the extracellular space has been performed both *in vivo* and *in vitro* in various protocols ranging from preventing lesion-induced spine loss (McKinney *et al.*, 1999) and quantifying internalization of AMPA receptors (Biou *et al.*, 2008) to inducing alterations of behaviors or of circadian rhythms (Mizoro *et al.*, 2010; Choi *et al.*, 2011). Obviously, we did not know (i) the exact AMPA concentration reaching the synaptic cleft and (ii) to what extent AMPA also acted at the extra-synaptic level in our conditions. In addition, there is a large diversity in the kinetics and permeability of AMPA receptors located on neocortical non-pyramidal cells (fast or slow desensitization and recovery, e.g. see Angulo *et al.*, 1997). However, we observed a clear increase in firing rate during spontaneous and evoked activity, indicating a depolarizing effect on cortical cells. Because we have recorded multi-unit activity composed of 3-6 cells, we cannot be sure that all cell types were equally excited by the AMPA and GBZ application, but the net output of small clusters of cortical neurons in terms of firing rate was equivalent after GBZ and AMPA application.

In our pilot studies, the lack of effect of TBOA application was surprising (see Methods) and we did not find satisfactory explanation for this puzzling result. Several *in vitro* studies have reported that this inhibitor increased post-synaptic currents in various brain structures (cerebellum: Crepel & Daniel, 2007; prefrontal cortex: Lambe & Aghajanian, 2007; hippocampus: Arnth-Jensen *et al.*, 2002) and increased the neuronal firing rate in the enthorinal cortex (Unichenko *et al.*, 2015). *In vivo*, cannula infusion of TBOA (100µM) induced a 120% increase in extrasynaptic glutamate concentration in the prefrontal cortex of awake rats (Hascup *et al.*, 2010). In contrast, in the striatum, TBOA reverse dialyze did not increase the extracellular glutamate level (Halpin *et al.*, 2014), and significantly reduced the evoked responses in the olfactory bulb (Gurden *et al.*, 2006), thus suggesting a potential area specificity for the action of this antagonist. Despite the abundant use of TBOA through the literature, this inhibitor had not been used in the primary auditory cortex, limiting comparison with our study.

Potential mechanisms leading to differences between GBZ and AMPA application.

At first look, there was no striking difference between the effects triggered by reducing intracortical inhibition or by increasing excitatory inputs reaching auditory cortex neurons. The discriminative ability (quantified by MI) of cortical cells was enhanced in both cases. However, this enhancement in MI was much larger when attenuating inhibition and it was accompanied by a large increase in spike-timing reliability, which did not occur when boosting excitation. We propose here that the main difference between “reducing inhibition” and “increasing excitation” comes from the impact on the synchronization between cortical discharges (Figure 7). When reducing intracortical inhibition, there was a large increase of the synchronization of neuronal responses quantified by cross-correlations as well as noise and signal correlations (Figure 7B-D). Therefore, during presentation of each

vocalization, the thalamic and cortical excitatory inputs and the feed-forward inhibition were not only stronger, but also more synchronized between neurons leading to periods of intense activation followed by prolonged periods of reduced spiking activity. In contrast, when enhancing the excitatory drive, the excitatory inputs are not more synchronized leaving the average spike-timing reliability unchanged and promoting only a modest gain in discrimination performance. The idea that the level of inhibition controls the synchronization between cortical cells is not new: attenuation of inhibition and disfacilitation has long been suspected to be a crucial factor in seizure initiation (reviewed in Timofeev & Steriade, 2004). More generally, *in vivo* intracellular studies and computational modeling have shown that inhibition also provides the largest contribution to membrane potential fluctuations as attested by the fact that spikes are preferentially evoked by a drop of inhibitory conductance (Rudolph *et al.*, 2007; Baudot *et al.*, 2013).

Modelling the impact of AMPA and GBZ on neuronal activity

The model used here is based on a balanced recurrent network, settled in an asynchronous and irregular regime as observed *in vivo* (Okun & Lampl, 2008; Renart *et al.*, 2010). While numerous theoretical studies investigated the regulation of the excitatory/inhibitory balance (Turrigiano, 2003; Taub *et al.*, 2013) as well as its role in spiking networks (see Vogels *et al.*, 2005 for review), no modelling studies have tried to disentangle the respective contributions of excitation and inhibition on evoked cortical activity. In our model, we found that simulating the effects of AMPA as an additive current uniformly impacting all neurons in the network resulted in a global increase in firing rate during external stimulation, without increasing the synchrony of the responses. In contrast, simulating the GBZ effect as a multiplicative phenomenon impacting only the activated inhibitory synapses resulted both in an increase in firing rate and in responses synchronization. This suggests that the fine temporal interplay between excitation and inhibition converging onto the same target neurons is crucial, as already observed with feed-forward inhibition (Vogels *et al.*, 2011). Our results also point out the inhibition as a key factor controlling the network synchronous activity, as already suggested on a theoretical basis (Tiesinga & Sejnowski, 2004). Perturbations of the balance by either an increase in excitation or a decrease in inhibition can change the synchronization of the responses while keeping the same global firing rate. This opens up the possibility that these two distinct ways to change the excitatory/inhibitory balance operate in cortical networks to code sensory information in two different modes (Heinzle *et al.*, 2007).

The role of cortical inhibition in spike-timing precision

In the auditory, somatosensory and visual cortices, natural stimuli are encoded by highly precise and reproducible patterns of neuronal discharges (Gabernet *et al.*, 2005; Herikstad *et al.*, 2011; Baudot *et al.*, 2013; Gaucher *et al.*, 2013*a*) but the mechanisms leading to these highly organized spike patterns remain unknown. As already proposed in the visual cortex (Baudot *et al.*, 2013), it is not the global level of excitability that matters to have a highly precise temporal organization of spiking activity at presentation of natural stimuli. Rather, it is the tight temporal interplay between excitation and inhibition, which requires a precise synchronization between neuronal discharges. Cortical inhibition has been associated to diverse of roles in sensory processing (Hirsch, 2003; Wehr & Zador, 2003; Monier *et al.*, 2003; Wilent & Contreras, 2005; Haider *et al.*, 2010; Cardin *et al.*, 2010), but it now becomes obvious that, in a more general way, it is a key factor for spiking pattern precision in neuronal networks via its controls on the temporal interplay between excitation and inhibition (Wehr & Zador, 2005; Kumar & Ohana, 2008; Vogels & Abbott, 2009; Renart *et al.*, 2010; Kremkow *et al.*, 2010*b*, 2010*a*; Baudot *et al.*, 2013; Graupner & Reyes, 2013). Admittedly, other

mechanisms involved in controlling the excitability of cortical cells can also operate. For example, changes in intrinsic excitability play an important role in modulating cortical responsiveness following visual deprivation (Nataraj & Turrigiano, 2011). In line with these studies, our results show that that modulating cortical inhibition alters the temporal precision of patterns of neuronal discharge compared to modulating cortical excitation.

Physiological control of cortical inhibitions

In normal physiological situation, neuromodulatory systems can exert a global impact on the excitatory and inhibitory network at a time scale of minutes. Neuromodulators target both pyramidal cells and inhibitory interneurons (Acetylcholine: Metherate *et al.*, 1992; Alitto & Dan, 2012; Noradrenaline: Toussay *et al.*, 2013; Salgado *et al.*, 2016; Serotonin: Aznar *et al.*, 2003; Santana *et al.*, 2004; De Almeida & Mengod, 2007; García-Oscos *et al.*, 2015), often with opposite effects on neuronal activity depending on the type of receptor activated. In addition, different neuromodulatory systems interact with each other (Esteban *et al.*, 1996; Villégier *et al.*, 2003) leading to difficulties in predicting what can be the net effect a particular neuromodulator action on cortical activity (review in Edeline, 2012). However, several recent studies using optogenetic manipulations suggested that neuromodulators, which preferentially control a particular type of interneuron can influence behavioral performance. For example, in the prefrontal cortex, the activation of PV+ neurons by Acetylcholine was found to be necessary for novel object recognition and spatial working memory (Yi *et al.*, 2014). In the auditory cortex, there is yet no direct evidence that manipulating intracortical inhibition can lead to significant alterations in discriminative performance at the neural and behavioral level. In fact, recent results obtained with optogenetic manipulations of PV+ interneurons in auditory cortex suggested a complex situation: while correlations were found between neurometric and psychometric performances, suppressing PV+ cells could increase the behavioral discrimination threshold of only some animals. On the contrary, activating PV+ cells led to decreased thresholds for some animals and increased for others (Briguglio *et al.*, 2018). As suggested by Moore et al (2018), the variability of optogenetic manipulations on behavioral and/or cortical thresholds can be a function of the type of pyramidal cells that are impacted by the activation/suppression of PV+ cells. In contrast with this latter study, the pharmacological manipulation used here via receptor antagonists or receptor agonists impacts the global excitability of the cortical network. Our results suggest that controlling the intracortical inhibition is probably the most efficient way to change the encoding capacity in auditory cortex. Further studies should now be designed to understand which type of cortical interneurons is required for these effects on the discrimination abilities of cortical cells.

Additional Information

Competing Interests

None declared.

Authors Contribution

This work has been performed at the Paris-Saclay Institute of Neurosciences (NeuroPSI). Q.G. and J-M.E. designed the experiments. Q.G. performed the experiment. Q.G. and P.Y. analyzed the data. J-M. E, Q.G. and P.Y. wrote the manuscript. All authors approved the final version of the manuscript.

Funding

This work was supported by grants from the National Research Agency (ANR Blanc2011-2014, HearFin and ANR Blanc2014-2018, HEART) to JME. QG was supported by a fellowship from the Ministère de l'Education Nationale et de la Recherche (MENR).

Acknowledgements

Special thanks to Fabien Lhericel and Céline Dubois for taking care of the guinea-pig colony.

Data Availability Statement

The data that support the findings of this study are available from the corresponding author upon reasonable request

References

Alitto HJ & Dan Y (2012). Cell-type-specific modulation of neocortical activity by basal forebrain input. *Front Syst Neurosci* **6,** 1–12.

De Almeida J & Mengod G (2007). Quantitative analysis of glutamatergic and GABAergic neurons expressing 5-HT2A receptors in human and monkey prefrontal cortex. *J Neurochem* **103,** 475–486.

Angulo MC, Lambolez B, Audinat E, Hestrin S & Rossier J (1997). Subunit Composition, Kinetic, and Permeation Properties of AMPA Receptors in Single Neocortical Nonpyramidal Cells. *J Neurosci* **17,** 6685–6696.

Arnth-Jensen N, Jabaudon D & Scanziani M (2002). Cooperation between independent hippocampal synapses is controlled by glutamate uptake. *Nat Neurosci* **5,** 325–331.

Averbeck BB, Latham PE & Pouget A (2006). Neural correlations, population coding and computation. *Nat Rev Neurosci* **7,** 358–366.

Averbeck BB & Lee D (2003). Neural noise and movement-related codes in the macaque supplementary motor area. *J Neurosci* **23,** 7630–7641.

Aznar S, Qian Z, Shah R, Rahbek B & Knudsen GM (2003). The 5-HT1A serotonin receptor is located on calbindin- and parvalbumin-containing neurons in the rat brain. *Brain Res* **959,** 58–67.

Baudot P, Levy M, Marre O, Monier C, Pananceau M & Frégnac Y (2013). Animation of natural scene by virtual eye-movements evokes high precision and low noise in V1 neurons. *Front Neural Circuits* **7,** 206.

Biou V, Bhattacharyya S & Malenka RC (2008). Endocytosis and recycling of AMPA receptors lacking GluR2/3. *Proc Natl Acad Sci U S A* **105,** 1038–1043.

Briguglio JJ, Aizenberg M, Balasubramanian V & Geffen MN (2018). Cortical Neural Activity Predicts Sensory Acuity Under Optogenetic Manipulation. *J Neurosci* **38,** 2094–2105.

Caesar K, Offenhauser N & Lauritzen M (2008). Gamma-aminobutyric acid modulates local brain oxygen consumption and blood flow in rat cerebellar cortex. *J Cereb Blood Flow Metab Off J Int Soc Cereb Blood Flow Metab* **28,** 906–915.

Caesar K, Thomsen K & Lauritzen M (2003). Dissociation of spikes, synaptic activity, and activity-dependent increments in rat cerebellar blood flow by tonic synaptic inhibition. *Proc Natl Acad Sci U S A* **100,** 16000–16005.

Cardin JA, Kumbhani RD, Contreras D & Palmer LA (2010). Cellular Mechanisms of Temporal Sensitivity in Visual Cortex Neurons. *J Neurosci* **30,** 3652–3662.

de Cheveigné A, Edeline J-M, Gaucher Q & Gourévitch B (2013). Component analysis reveals sharp tuning of the local field potential in the guinea pig auditory cortex. *J Neurophysiol* **109,** 261–272.

Choi KH, Edwards S, Graham DL, Larson EB, Whisler KN, Simmons D, Friedman AK, Walsh JJ, Rahman Z, Monteggia LM, Eisch AJ, Neve RL, Nestler EJ, Han MH & Self DW (2011). Reinforcement-related regulation of AMPA glutamate receptor subunits in the ventral tegmental area enhances motivation for cocaine. *J Neurosci* **31,** 7927–7937.

Crepel F & Daniel H (2007). Developmental changes in agonist-induced retrograde signaling at parallel fiber-Purkinje cell synapses: role of calcium-induced calcium release. *J Neurophysiol* **98,** 2550–2565.

Darbin O, Newton L & Wichmann T (2006). A new probe to monitor the effects of drugs on local field potentials. *J Neurosci Methods* **155,** 291–295.

Darbin O & Wichmann T (2008). Effects of striatal GABA A-receptor blockade on striatal and cortical activity in monkeys. *J Neurophysiol* **99,** 1294–1305.

Debanne D & Poo MM (2010). Spike-timing dependent plasticity beyond synapse - pre- and post-synaptic plasticity of intrinsic neuronal excitability. *Front Synaptic Neurosci* **2,** 1–6.

Destexhe A, Contreras D, Steriade M. (1999) Cortically-induced coherence of a thalamic-generated

oscillation. Neuroscience ;92(2):427-43.
Edeline J-M (2012). Beyond traditional approaches to understanding the functional role of neuromodulators in sensory cortices. *Front Behav Neurosci* **6,** 1–14.
Edeline JM, Dutrieux G, Manunta Y & Hennevin E (2001). Diversity of receptive field changes in auditory cortex during natural sleep. *Eur J Neurosci* **14,** 1865–1880.
Edeline JM & Weinberger NM (1993). Receptive field plasticity in the auditory cortex during frequency discrimination training: selective retuning independent of task difficulty. *Behav Neurosci* **107,** 82–103.
Esteban S, Lladó J & García-Sevilla JA (1996). Alpha 2-autoreceptors and alpha 2-heteroreceptors modulating tyrosine and tryptophan hydroxylase activity in the rat brain in vivo: an investigation into the alpha 2-adrenoceptor subtypes. *Naunyn Schmiedebergs Arch Pharmacol* **353,** 391–399.
Froemke RC, Merzenich MM & Schreiner CE (2007). A synaptic memory trace for cortical receptive field plasticity. *Nature* **450,** 425–429.
Gabernet L, Jadhav SP, Feldman DE, Carandini M & Scanziani M (2005). Somatosensory Integration Controlled by Dynamic Thalamocortical Feed-Forward Inhibition. *Neuron* **48,** 315–327.
García-Oscos F, Torres-Ramírez O, Dinh L, Galindo-Charles L, Pérez Padilla EA, Pineda JC, Atzori M & Salgado H (2015). Activation of 5-HT receptors inhibits GABAergic transmission by pre-and post-synaptic mechanisms in layer II/III of the juvenile rat auditory cortex. *Synapse* **69,** 115–127.
Gaucher Q & Edeline J-M (2015). Stimulus-specific effects of noradrenaline in auditory cortex: implications for the discrimination of communication sounds. *J Physiol* **593,** 1003–1020.
Gaucher Q, Edeline JM & Gourévitch B (2012). How different are the local field potentials and spiking activities? Insights from multi-electrodes arrays. *J Physiol Paris* **106,** 93–103.
Gaucher Q, Huetz C, Gourévitch B & Edeline J-M (2013*a*). Cortical inhibition reduces information redundancy at presentation of communication sounds in the primary auditory cortex. *J Neurosci* **33,** 10713–10728.
Gaucher Q, Huetz C, Gourévitch B, Laudanski J, Occelli F & Edeline J-M (2013*b*). How do auditory cortex neurons represent communication sounds? *Hear Res* **305,** 102–112.
Gourévitch B, Doisy T, Avillac M & Edeline JM (2009). Follow-up of latency and threshold shifts of auditory brainstem responses after single and interrupted acoustic trauma in guinea pig. *Brain Res* **1304,** 66–79.
Gourévitch B & Edeline J-M (2011). Age-related changes in the guinea pig auditory cortex: relationship with brainstem changes and comparison with tone-induced hearing loss. *Eur J Neurosci* **34,** 1953–1965.
Graupner M & Reyes AD (2013). Synaptic Input Correlations Leading to Membrane Potential Decorrelation of Spontaneous Activity in Cortex. *J Neurosci* **33,** 15075–15085.
Gurden H, Uchida N & Mainen ZF (2006). Sensory-Evoked Intrinsic Optical Signals in the Olfactory Bulb Are Coupled to Glutamate Release and Uptake. *Neuron* **52,** 335–345.
Haider B, Krause MR, Duque A, Yu Y, Touryan J, Mazer JA & McCormick DA (2010). Synaptic and Network Mechanisms of Sparse and Reliable Visual Cortical Activity during Nonclassical Receptive Field Stimulation. *Neuron* **65,** 107–121.
Halpin LE, Northrop NA & Yamamoto BK (2014). Ammonia mediates methamphetamine-induced increases in glutamate and excitotoxicity. *Neuropsychopharmacology* **39,** 1031–1038.
Hascup ER, Hascup KN, Stephens M, Pomerleau F, Huettl P, Gratton A & Gerhardt GA (2010). Rapid microelectrode measurements and the origin and regulation of extracellular glutamate in rat prefrontal cortex. *J Neurochem* **115,** 1608–1620.
Heinzle J, König P & Salazar RF (2007). Modulation of synchrony without changes in firing rates. *Cogn Neurodyn* **1,** 225–235.
Hensch TK & Fagiolini M (2005). Excitatory–inhibitory balance and critical period plasticity in developing visual cortex. *Prog Brain Res* **147,** 115–124.

Herikstad R, Baker J, Lachaux J-P, Gray CM & Yen S-C (2011). Natural movies evoke spike trains with low spike time variability in cat primary visual cortex. *J Neurosci Off J Soc Neurosci* **31,** 15844–15860.

Hirsch JA (2003). Synaptic physiology and receptive field structure in the early visual pathway of the cat. *Cereb Cortex (New York, NY 1991)* **13,** 63–69.

Huetz C, Philibert B & Edeline J-MM (2009). A spike-timing code for discriminating conspecific vocalizations in the thalamocortical system of anesthetized and awake guinea pigs. *J Neurosci* **29,** 334–350.

Isaacson JS & Scanziani M (2011). How Inhibition Shapes Cortical Activity. *Neuron* **72,** 231–243.

Jones MS & Barth DS (2002). Effects of Bicuculline Methiodide on Fast (>200 Hz) Electrical Oscillations in Rat Somatosensory Cortex. *J Neurophysiol* **88,** 1016–1025.

Kremkow J, Aertsen A & Kumar A (2010*a*). Gating of Signal Propagation in Spiking Neural Networks by Balanced and Correlated Excitation and Inhibition. *J Neurosci* **30,** 15760–15768.

Kremkow J, Perrinet LU, Masson GS & Aertsen A (2010*b*). Functional consequences of correlated excitatory and inhibitory conductances in cortical networks. *J Comput Neurosci* **28,** 579–594.

Kumar P & Ohana O (2008). Inter- and Intralaminar Subcircuits of Excitatory and Inhibitory Neurons in Layer 6a of the Rat Barrel Cortex. *J Neurophysiol* **100,** 1909–1922.

Lambe EK & Aghajanian GK (2007). Prefrontal cortical network activity: Opposite effects of psychedelic hallucinogens and D1/D5 dopamine receptor activation. *Neuroscience* **145,** 900–910.

Latham PE & Nirenberg S (2005). Synergy, redundancy, and independence in population codes, revisited. *J Neurosci* **25,** 5195–5206.

Li H, Liang F, Zhong W, Yan L, Mesik L, Xiao Z, Tao HW & Zhang LI (2019). Synaptic Mechanisms for Bandwidth Tuning in Awake Mouse Primary Auditory Cortex. *Cereb Cortex* **29,** 2998–3009.

Liang F, Li H, Chou X, Zhou M, Zhang NK, Xiao Z, Zhang KK, Tao HW & Zhang LI (2019). Sparse Representation in Awake Auditory Cortex: Cell-type Dependence, Synaptic Mechanisms, Developmental Emergence, and Modulation. *Cereb Cortex* **29,** 3796–3812.

Manunta Y & Edeline JM (1997). Effects of noradrenaline on frequency tuning of rat auditory cortex neurons. *Eur J Neurosci* **9,** 833–847.

Manunta Y & Edeline JM (1999). Effects of noradrenaline on frequency tuning of auditory cortex neurons during wakefulness and slow-wave sleep. *Eur J Neurosci* **11,** 2134–2150.

McKinney RA, Capogna M, Dürr R, Gähwiler BH & Thompson SM (1999). Miniature synaptic events maintain dendritic spines via AMPA receptor activation. *Nat Neurosci* **2,** 44–49.

Metherate R, Cox CL & Ashe JH (1992). Cellular bases of neocortical activation: modulation of neural oscillations by the nucleus basalis and endogenous acetylcholine. *J Neurosci Off J Soc Neurosci* **12,** 4701–4711.

Mizoro Y, Yamaguchi Y, Kitazawa R, Yamada H, Matsuo M, Fustin JM, Doi M & Okamura H (2010). Activation of AMPA receptors in the suprachiasmatic nucleus phase-shifts the mouse circadian clock in vivo and in vitro. *PLoS One* **5,** 2–7.

Monier C, Chavane F, Baudot P, Graham LJ & Frégnac Y (2003). Orientation and direction selectivity of synaptic inputs in visual cortical neurons: a diversity of combinations produces spike tuning. *Neuron* **37,** 663–680.

Moore AK & Wehr M (2013). Parvalbumin-Expressing Inhibitory Interneurons in Auditory Cortex Are Well-Tuned for Frequency. *J Neurosci* **33,** 13713–13723.

Moore AK, Weible AP, Balmer TS, Trussell LO & Wehr M (2018). Rapid Rebalancing of Excitation and Inhibition by Cortical Circuitry. *Neuron* **97,** 1341-1355.e6.

Nataraj K & Turrigiano G (2011). Regional and temporal specificity of intrinsic plasticity mechanisms in rodent primary visual cortex. *J Neurosci* **31,** 17932–17940.

Nelson SB & Turrigiano GG (2008). Strength through Diversity. *Neuron* **60,** 477–482.

Okun M & Lampl I (2008). Instantaneous correlation of excitation and inhibition during ongoing and sensory-evoked activities. *Nat Neurosci* **11,** 535–537.

Oswald A-MM, Schiff ML & Reyes AD (2006). Synaptic mechanisms underlying auditory processing. *Curr Opin Neurobiol* **16,** 371–376.

Pinaud R, Terleph TA, Tremere LA, Phan ML, Dagostin AA, Leao RM, Mello C V., Vicario DS, Leão RM, Mello C V. & Vicario DS (2008). Inhibitory Network Interactions Shape the Auditory Processing of Natural Communication Signals in the Songbird Auditory Forebrain. *J Neurophysiol* **100,** 441–455.

Renart A, de la Rocha J, Bartho P, Hollender L, Parga N, Reyes A & Harris KD (2010). The Asynchronous State in Cortical Circuits. *Science (80-)* **327,** 587–590.

Riquimaroux H, Gaioni SJ & Suga N (1991). Cortical computational maps control auditory perception. *Science* **251,** 565–568.

Riquimaroux H, Gaioni SJ & Suga N (1992). Inactivation of the DSCF area of the auditory cortex with muscimol disrupts frequency discrimination in the mustached bat. *J Neurophysiol* **68,** 1613–1623.

Robertson D & Irvine DR (1989). Plasticity of frequency organization in auditory cortex of guinea pigs with partial unilateral deafness. *J Comp Neurol* **282,** 456–471.

Rosen MJ & Mooney R (2003). Inhibitory and excitatory mechanisms underlying auditory responses to learned vocalizations in the songbird nucleus HVC. *Neuron* **39,** 177–194.

Rudolph M, Pospischil M, Timofeev I & Destexhe A (2007). Inhibition determines membrane potential dynamics and controls action potential generation in awake and sleeping cat cortex. *J Neurosci* **27,** 5280–5290.

Salgado H, Treviño M & Atzori M (2016). Layer- and area-specific actions of norepinephrine on cortical synaptic transmission. *Brain Res* **1641,** 163–176.

Santana N, Bortolozzi A, Serrats J, Mengod G & Artigas F (2004). Expression of serotonin1A and serotonin2A receptors in pyramidal and GABAergic neurons of the rat prefrontal cortex. *Cereb Cortex* **14,** 1100–1109.

Schnupp JWH (2006). Plasticity of Temporal Pattern Codes for Vocalization Stimuli in Primary Auditory Cortex. *J Neurosci* **26,** 4785–4795.

Shannon CE (1948). A Mathematical Theory of Communication. *Bell Syst Tech J* **27,** 379–423.

Shimamoto K, Lebrun B, Yasuda-Kamatani Y, Sakaitani M, Shigeri Y, Yumoto N & Nakajima T (1998). DL-threo-beta-benzyloxyaspartate, a potent blocker of excitatory amino acid transporters. *Mol Pharmacol* **53,** 195–201.

Swadlow HA (2003). Fast-spike interneurons and feedforward inhibition in awake sensory neocortex. *Cereb Cortex (New York, NY 1991)* **13,** 25–32.

Tachibana Y, Kita H, Chiken S, Takada M & Nambu A (2008). Motor cortical control of internal pallidal activity through glutamatergic and GABAergic inputs in awake monkeys. *Eur J Neurosci* **27,** 238–253.

Tan AYY & Wehr M (2009). Balanced tone-evoked synaptic excitation and inhibition in mouse auditory cortex. *Neuroscience* **163,** 1302–1315.

Taub AH, Katz Y & Lampl I (2013). Cortical balance of excitation and inhibition is regulated by the rate of synaptic activity. *J Neurosci* **33,** 14359–14368.

Tiesinga PHE & Sejnowski TJ (2004). Rapid Temporal Modulation of Synchrony by Competition in Cortical Interneuron Networks. *Neurocomputing* **65–66,** 809–815.

Timofeev I & Steriade M (2004). Neocortical seizures: Initiation, development and cessation. *Neuroscience* **123,** 299–336.

Toussay X, Basu K, Lacoste B & Hamel E (2013). Locus coeruleus stimulation recruits a broad cortical neuronal network and increases cortical perfusion. *J Neurosci* **33,** 3390–3401.

Turrigiano G (2003). Homeostatic Regulation of Excitatory-Inhibitory Balance. In *Excitatory-Inhibitory Balance*, pp. 187–195. Springer US, Boston, MA.

Turrigiano GG & Nelson SB (2000). Hebb and homeostasis in neuronal plasticity. *Curr Opin Neurobiol* **10,** 358–364.

Turrigiano GG & Nelson SB (2004). Homeostatic plasticity in the developing nervous system. *Nat Rev*

Neurosci **5,** 97–107.
Unichenko P, Yang JW, Luhmann HJ & Kirischuk S (2015). Glutamatergic system controls synchronization of spontaneous neuronal activity in the murine neonatal entorhinal cortex. *Pflugers Arch Eur J Physiol* **467,** 1565–1575.
Villégier A-S, Drouin C, Bizot J-C, Marien M, Glowinski J, Colpaërt F & Tassin J-P (2003). Stimulation of postsynaptic alpha1b- and alpha2-adrenergic receptors amplifies dopamine-mediated locomotor activity in both rats and mice. *Synapse* **50,** 277–284.
Vogels TP & Abbott LF (2009). Gating multiple signals through detailed balance of excitation and inhibition in spiking networks. *Nat Neurosci* **12,** 483–491.
Vogels TP, Rajan K & Abbott LF (2005). Neural Network Dynamics. *Annu Rev Neurosci* **28,** 357–376.
Vogels TP, Sprekeler H, Zenke F, Clopath C & Gerstner W (2011). Inhibitory plasticity balances excitation and inhibition in sensory pathways and memory networks. *Science* **334,** 1569–1573.
Wallace MN & Palmer AR (2007). Laminar differences in the response properties of cells in the primary auditory cortex. *Exp Brain Res* **184,** 179–191.
Wallace MN, Rutkowski RG & Palmer AR (2000). Identification and localisation of auditory areas in guinea pig cortex. *Exp Brain Res* **132,** 445–456.
Wang H, Turner JG, Ling L, Parrish JL, Hughes LF & Caspary DM (2009*a*). Age-related changes in glycine receptor subunit composition and binding in dorsal cochlear nucleus. *Neuroscience* **160,** 227–239.
Wang X (2018). Cortical Coding of Auditory Features. *Annu Rev Neurosci* **41,** 527–552.
Wang X, Chen G, Gao W & Ebner T (2009*b*). Long-term potentiation of the responses to parallel fiber stimulation in mouse cerebellar cortex in vivo. *Neuroscience* **162,** 713–722.
Wehr M & Zador AM (2003). Balanced inhibition underlies tuning and sharpens spike timing in auditory cortex. *Nature* **426,** 442–446.
Wehr M & Zador AM (2005). Synaptic mechanisms of forward suppression in rat auditory cortex. *Neuron* **47,** 437–445.
Wilent WB & Contreras D (2005). Dynamics of excitation and inhibition underlying stimulus selectivity in rat somatosensory cortex. *Nat Neurosci* **8,** 1364–1370.
Wu GK, Arbuckle R, Liu B, Tao HW & Zhang LI (2008). Lateral Sharpening of Cortical Frequency Tuning by Approximately Balanced Inhibition. *Neuron* **58,** 132–143.
Xue M, Atallah B V. & Scanziani M (2014). Equalizing excitation–inhibition ratios across visual cortical neurons. *Nature* **511,** 596–600.
Yi F, Ball J, Stoll KE, Satpute VC, Mitchell SM, Pauli JL, Holloway BB, Johnston AD, Nathanson NM, Deisseroth K, Gerber DJ, Tonegawa S & Lawrence JJ (2014). Direct excitation of parvalbumin-positive interneurons by M 1 muscarinic acetylcholine receptors: roles in cellular excitability, inhibitory transmission and cognition. *J Physiol* **592,** 3463–3494.
Yizhar O, Fenno LE, Prigge M, Schneider F, Davidson TJ, O'Shea DJ, Sohal VS, Goshen I, Finkelstein J, Paz JT, Stehfest K, Fudim R, Ramakrishnan C, Huguenard JR, Hegemann P & Deisseroth K (2011). Neocortical excitation/inhibition balance in information processing and social dysfunction. *Nature* **477,** 171–178.
Yu H, Chen X, Sun C & Shou T (2008). Global evaluation of contributions of GABA A, AMPA and NMDA receptors to orientation maps in cat's visual cortex. *Neuroimage* **40,** 776–787.

Figure legends

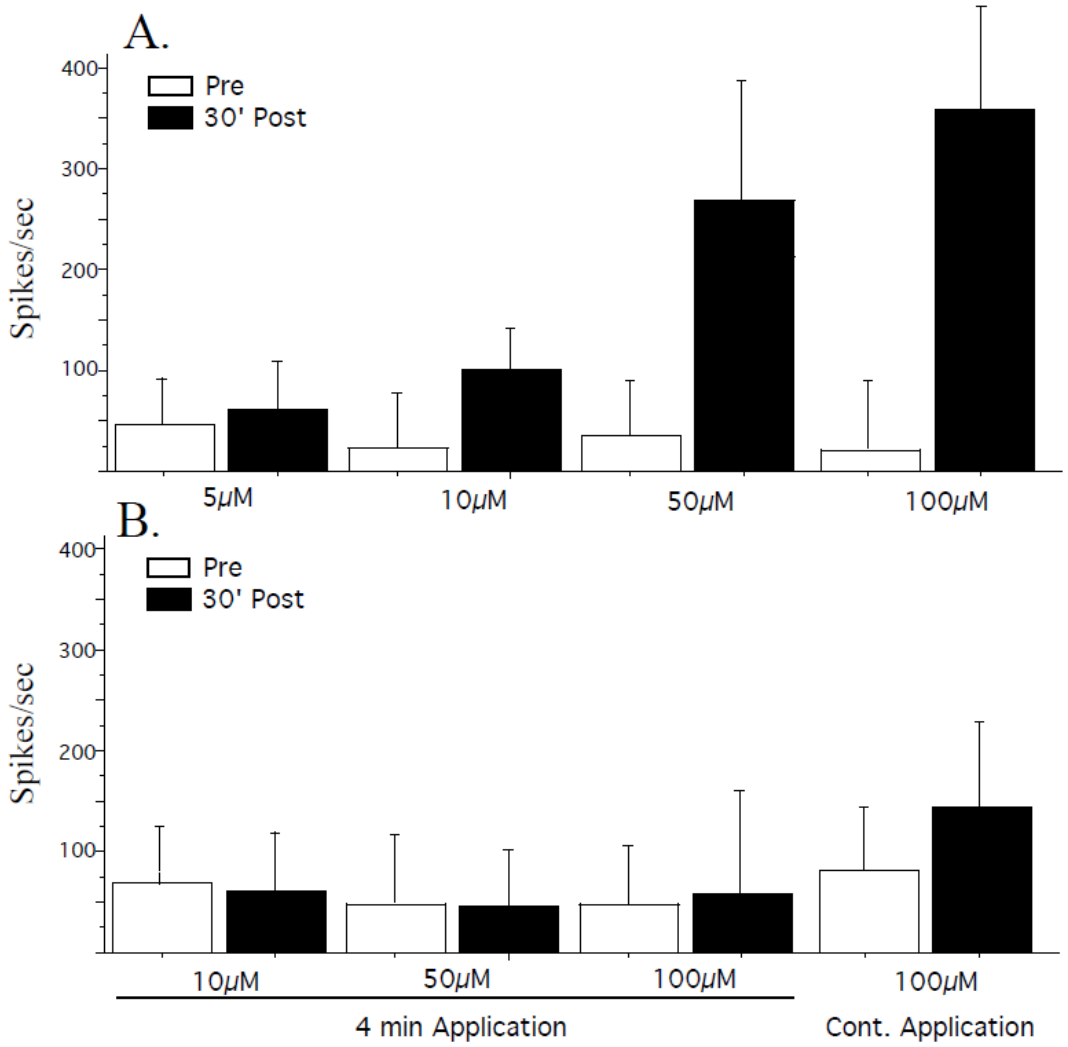

Figure 1: Dose-response quantifications for AMPA and GBZ. The strength of evoked responses to pure tones (mean ± SD) were quantified from STRFs measured every 6 minutes at 75dB SPL after application. **A.** For GBZ application, we tested 4-minute applications at different concentrations of GBZ. Both the 100 and the 50 µM concentrations produced very large increases in evoked responses but epileptic seizure-like activity was detected in several occasions. At 5 µM we did not detect significant increase in evoked responses. A 10 µM concentration triggered consistent and significant increases of the evoked responses. **B.** For AMPA application, we tested 4-minute applications from 10 µM up to 100 µM without obtaining significant effects on the strength of evoked responses. A continuous application at 100 µM produced a significant increase in evoked responses without triggering epileptic seizure-like activity. Based on these dose-responses curves, we used a 4-minute application of GBZ at 10 µM and a continuous application of AMPA at 100 µM in the rest of our experiments.

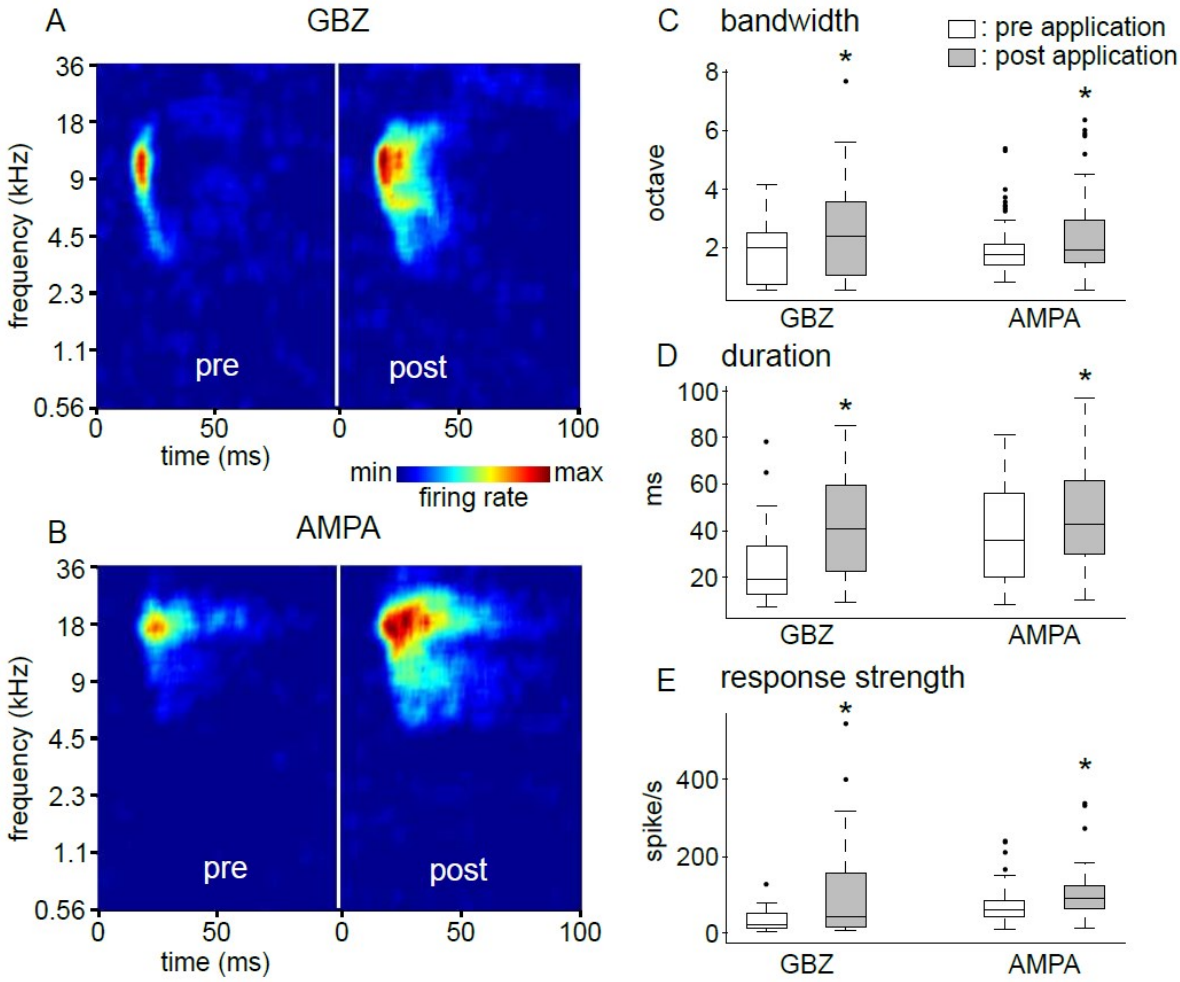

Figure 2. Effects of GBZ and AMPA on Spectro-Temporal Receptive Fields (STRFs)

Examples of typical STRFs obtained before and after GBZ (**A**) and AMPA (**B**) application. Effects of GBZ and AMPA application on the bandwidth (**C**), duration (**D**) and response strength (**E**) of STRFs. Central mark: median; bottom and top of the box: 25th and 75th percentiles; whiskers: ±2.7σ; black dots: outliers. White boxes: prior to application, grey boxes: post application. *: $p<0.05$, Wilcoxon signed-rank test.

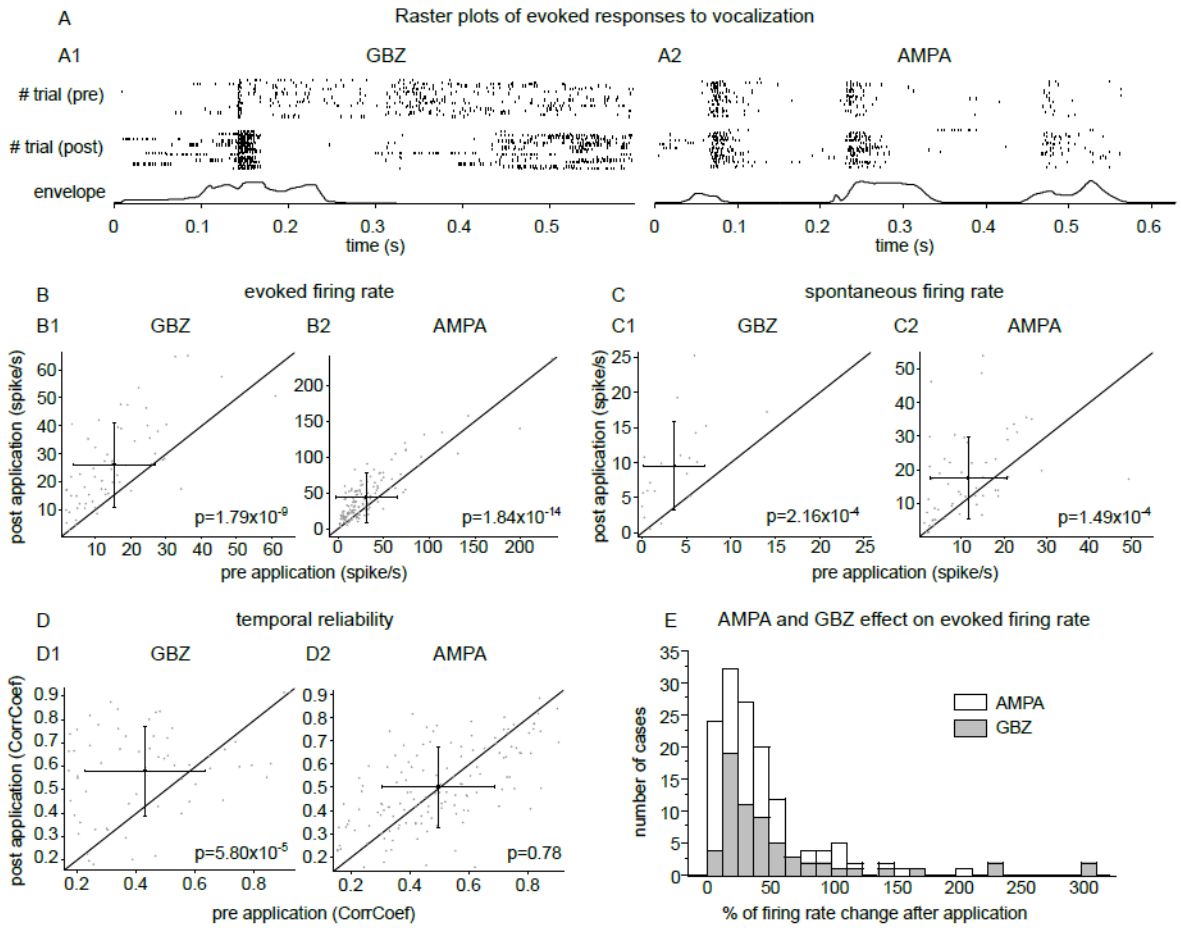

Figure 3. Effects of GBZ and AMPA on responses to vocalizations and spontaneous activity.

A. Raster plots of evoked responses to one vocalization before (top panel) and after (middle panel) drug application. The temporal envelope of each vocalization is presented in the bottom panel. **B.** Scatter plots showing the effects of GBZ (**B1**) and AMPA (**B2**) application on evoked firing rate. **C.** Scatter plots showing the effects of GBZ (**C1**) and AMPA (**C2**) application on temporal reliability (CorrCoef) during the response to vocalizations. **D.** Scatter plots showing the effects of GBZ (**D1**) and AMPA (**D2**) application on spontaneous activity (**C**). Black cross: mean ± SD. p-values: Wilcoxon signed rank test between pre and post application conditions. **D.** Distributions of the percentage of change in evoked activity obtained after GBZ and AMPA application. These distributions are not different (Chi-square, p=0.37).

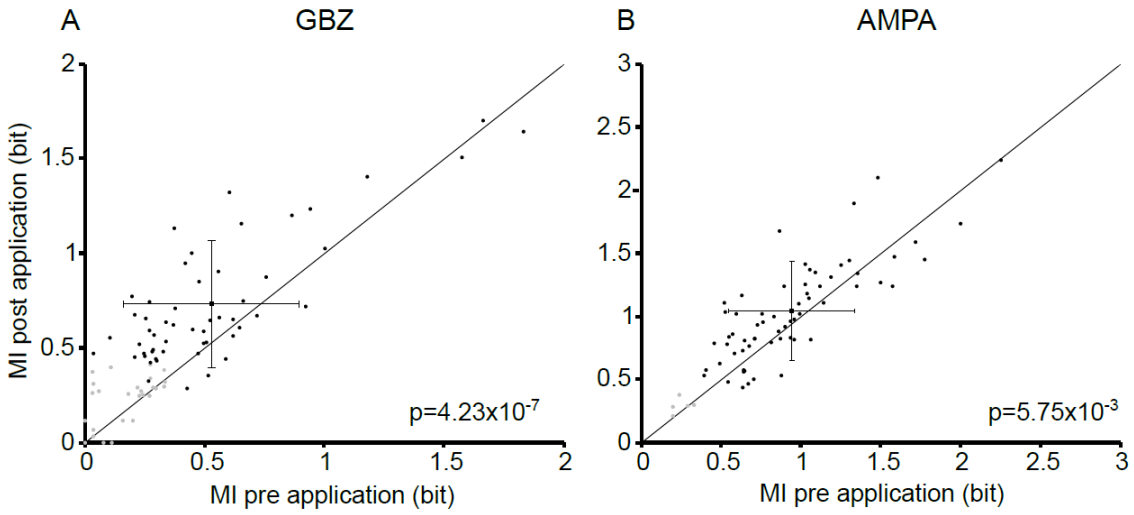

Figure 4. Mutual Information (MI) carried by responses to vocalizations before and after drug application.

A. Scatter plot showing the MI carried by the cortical recordings before and after GBZ application. **B.** Scatter plot showing the MI carried by the cortical recordings before and after AMPA application. The MI is based on temporal spike patterns ($MI_{Patterns}$, see Methods). Gray dots represent non-significant values of MI (see Methods). Black cross: mean ± SD of significant MI values. p-values: Wilcoxon signed rank test between pre and post application conditions.

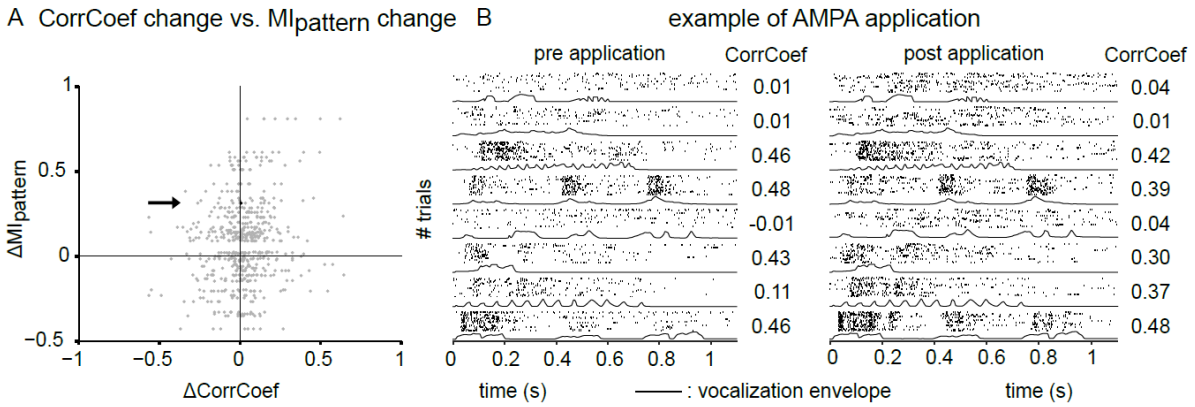

Figure 5. Comparison between AMPA effects on the MI and on the CorrCoef.

A. Scatter plot displaying the CorrCoef variation versus the MI variation induced by AMPA application. The MI value is computed for each cortical recording whereas the CorrCoef value is computed for each vocalization, so each MI value corresponds to eight values of CorrCoef. The black dot represents the average CorrCoef value for one recording site example (see B.). Black arrow: individual example shown in B. **B.** Raster plots of evoked responses to the eight vocalizations before (left panel) and after (right panel) AMPA application. The temporal envelope of each vocalization is presented at the bottom of each raster plot (black lines).

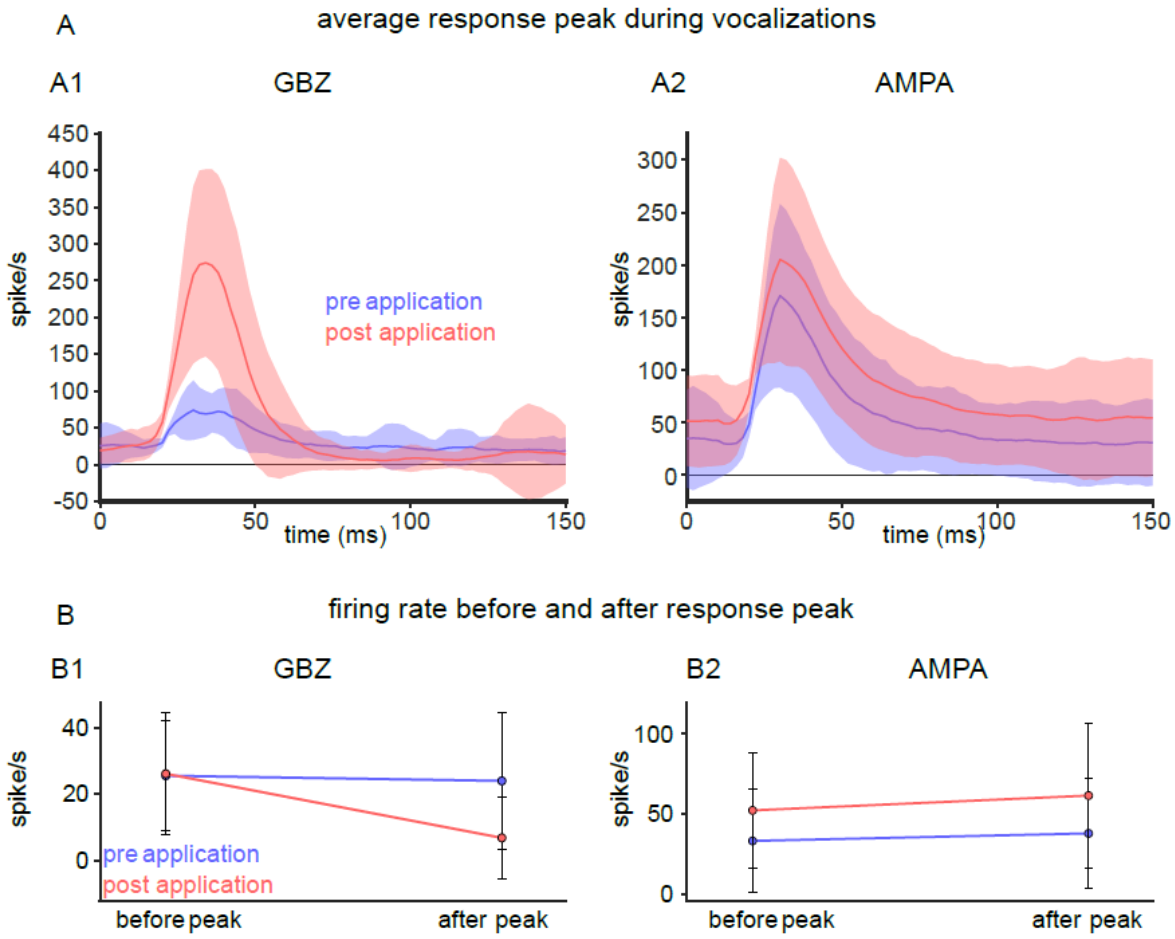

Figure 6. Effects of GBZ and AMPA on the phasic peaks of response within the PSTHs.

A. Averaged significant peaks of response occurring within the PSTHs of cortical response to vocalizations. These peaks were averaged before and after GBZ (A1) and AMPA (A2) applications. Blue trace: before application; red trace: after application; colored shade: standard error. **B.** Mean ± SD values of firing rate obtained before and after the peaks after GBZ (B1) or AMPA (B2) application. Blue trace: before application; red trace: after application.

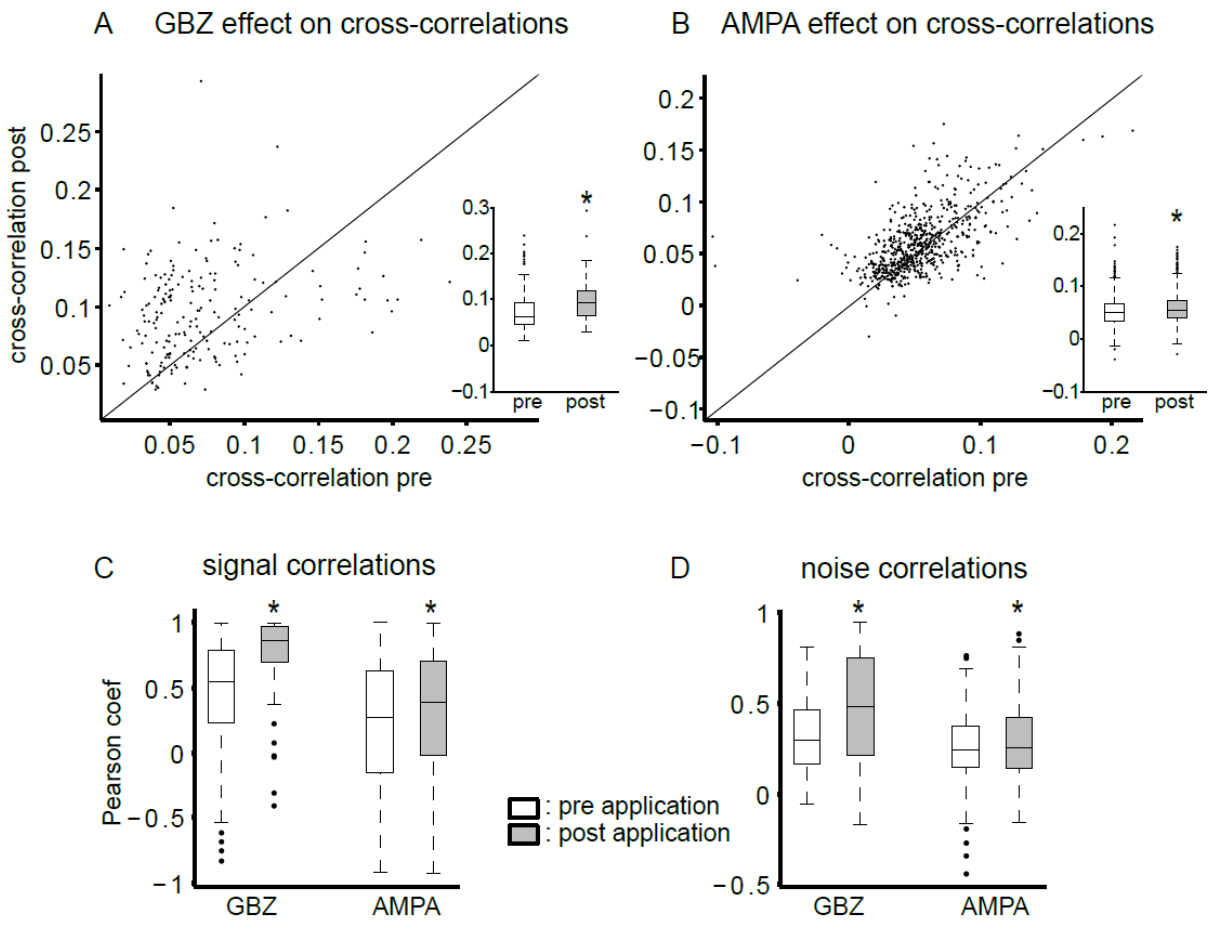

Figure 7. Effects of GBZ and AMPA on the cross-correlations, noise and signal correlations.

A. Scatterplots displaying the maximum level of cross-correlation (during evoked activity) between simultaneous cortical recordings before and after GBZ application. **B.** Same before and after AMPA application. Inset box plot: cross-correlation values before (white box) and after (grey box) drug application. **C.** Signal correlation during responses to vocalizations before (white box) and after (grey box) GBZ and AMPA application. **D.** Same for noise correlations. Central mark: median; bottom and top of the box: 25th and 75th percentiles; whiskers: ±2.7σ; black dots: outliers. *: $p<0.05$, Wilcoxon signed-rank test.

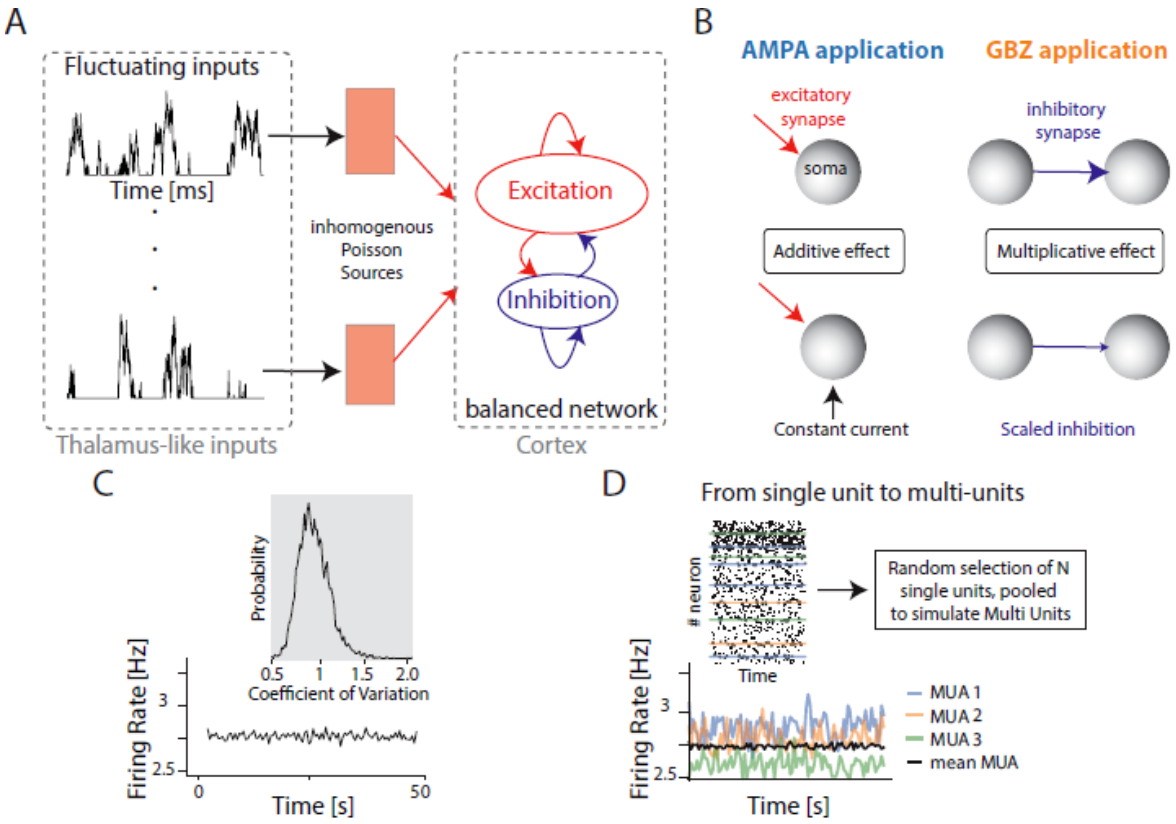

Figure 8. Schematic diagram of the feed-forward model used for analyzing the effects of AMPA and GBZ application

A. Eight groups of inhomogeneous Poisson sources (excitatory and inhibitory) were used to stimulate neurons in a feed-forward manner. Each of those groups is fed with a fluctuating input, with a maximum amplitude of 100Hz. **B.** The effect of AMPA application onto the cortex is modeled as an additive effect, by a constant depolarizing current injected into all neurons. On the opposite, Gabazine (GBZ) application is modeled as a multiplicative scaling of all the inhibitory weights. **C.** Spontaneous firing rate of the balanced network, when no inputs are presented, showing an Asynchronous Irregular regime at 2.5 Hz. Inset shows the distribution of the coefficient of variation for the inter spike intervals, with a mean close to 1. **D.** Generation of artificial Multi Unit activity (MU) to compare to experimental data. Between 1 and 5 neurons are randomly selected within the network to create a fake MU by combining all their spikes.

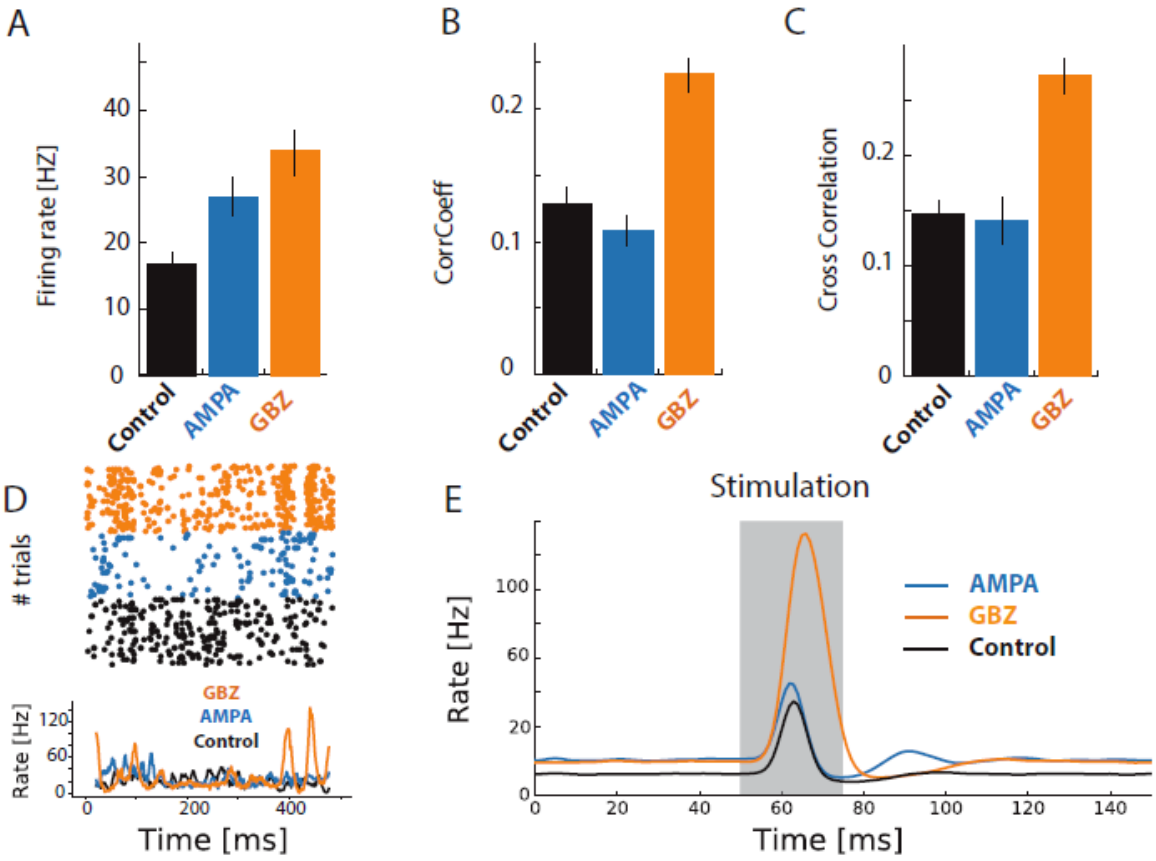

Figure 9. The feed-forward model reproduces the increase of synchronization observed during GBZ Application.

A. Average firing rate (± SD) of the network in response to the same external inputs either in control condition (black), after AMPA application (blue), or after GBZ application (orange). **B.** Average correlation coefficient (CorrCoef) between trials (± SD), for 50 input patterns, each of them repeated 100 times (see Methods), for the three cases explained in **A. C.** Average values of Cross Correlation between neuronal discharges (± SD), computed at time 0. **D.** Top, raster plot showing the responses of simulated MU within the network when the same input pattern is presented, for the three different conditions shown in **A.** (every line is a cell). Bottom shows the average firing rate for this particular pattern, averaged over a population of 1000 MUs. Note the large variability observed when the balanced is perturbed multiplicatively (GBZ application, orange curve). **E.** Averaged responses over 100 neurons and 500 presentations of random vocalizations, either in control condition (black), after AMPA application (blue), or after GBZ application (orange). Note the qualitative difference in the PSTH shapes as in the physiological data (Figure 6): the post excitation suppression was observed after GBZ application but not after AMPA application.

Quentin Gaucher completed his PhD in France (Paris-Saclay Institute of Neuroscience) under the supervision of Jean-Marc Edeline and is currently part of the Walker's group (Department of Physiology, Anatomy and Genetics, University of Oxford). His main research interest is auditory neuroscience, with a focus on the auditory cortex and acoustic communication. His past project investigated how the balance of activity between excitatory and inhibitory neurons controls their responses to communication calls in guinea pigs. He currently works the cortical processes underlying the perception of pitch in ferrets and mice, using calcium imaging and electrophysiology.